Programmable shape morphing and space deployment through graded derivatives of origami architectures

A. Sharma[a], S. Naskar[a], T. Mukhopadhyay[a,*]

[a]*Faculty of Engineering and Physical Sciences, University of Southampton, Southampton, UK*

Abstract

Real-time programmable mechanical features including shape morphing ability in metamaterials and metasurfaces can be crucial for a range of technologically demanding space applications such as deployable space structures and antennas, adaptive solar arrays, robotic arms, actuators and advanced robotic materials. This paper proposes second-order derivatives of spatially-varying Miura-based origami architectures like graded Arc Miura, inclined Arc Miura, and tapered Arc Miura for achieving a range of programmable shape-changing capabilities. The rigid foldability and motion behavior of the graded geometries are investigated thoroughly based on computational simulations and tabletop experiments using physical prototypes, leading to the evidence of on-demand shape morphing and target curvature attainment under limited actuation, and transitional deployment from 2D to 3D states. An efficient approach of kinematic mapping is developed based on idealized spherical 4R linkages involving Denavit-Hartenberg matrix notations, resulting in piece-wise spatially-graded tessellations for achieving programmed pre-defined symmetric and asymmetric curvatures with complex two and three-dimensional geometrical shapes. The fundamental mechanics of the proposed origami metamaterials being mostly scale-independent, this emerging class of deployable shape-changing architectures can be directly transferred for application in a range of milli-, micro-, and nano-metre-size space systems, essentially opening avenues for the design of various programmable structures and machines at multiple length-scales.

Keywords: Shape morphing and deployment; Origami derivatives; Programmable metamaterials and metasurfaces; Spatially-graded origami architectures; Helical origami

1. Introduction

Origami, the Japanese art of folding paper into a variety of three-dimensional shapes, has inspired a rapidly growing branch of science and engineering that specializes in the manufacture of three-dimensional engineering structures from initially two-dimensional pre-forms through fold-like processes (i.e. 2D to 3D state-transition). While the word "origami" comes from the Japanese origins for "folded" (ori) and "paper" (kami), the folding concepts of origami can be extended readily to other advanced materials suited for critical engineering applications. Origami is a technique that can be thought of as a process in which a large flat piece of material is folded in a pre-set way to form a particular target shape that is compact, possibly rigid, deployable and portable, or sometimes produces a target motion behavior, depending on the intended applications.

*Corresponding author: Tanmoy Mukhopadhyay (Email address: T.Mukhopadhyay@soton.ac.uk)

The general field of deployable structures include various structural systems and mechanics such as origami and kirigami, bar-hinge mechanisms, tensegrity and inflatable structures [1–6]. Different space mechanisms and structures can be adopted based on application specific demands, analyzing the associated advantages and disadvantages. For example, tensegrity structures are composed of a set of discontinuous compression bars and continuous cables in a self-balancing space grid structure. This unique design makes them lightweight while maintaining stiffness. Furthermore, the stiffness, shape control and equilibrium states of tensegrity structures can be precisely controlled by altering the string parameters. However, these structures are inherently complex due to complicated joints, where each compression bar interacts with several other bars, requiring various degrees of freedom for proper assembly and functionality [7, 8]. Origami architectures on the other hand rely on the foldable crease pattern for their intrinsic stability and functionalities [6, 9, 10]. The foldable crease patterns of origami structures offer a range of advanced functionalities including compact storage, predictable deformation, multistability, complex shape attainment, negative Poisson's ratio and lightweight design. Additionally, origami structures can fold and unfold through limited actuation requirements with better control, significantly simplifying the automated deployment and storage mechanism. Such advantages make origami-based architectures suitable for space applications. Over the recent years, origami folding patterns have been widely adopted in a range of technologically demanding applications such as mechanical metamaterials and metasurfaces [1, 11–19], nanomaterials [20–22], soft robotics [23–26], rotorcraft [27], energy absorbing protective structures and sandwich cores [28, 29], energy harvesters [30], antennas [31], and large-scale space structures [32–34]. The focus of this article is to achieve programmable state-transitional shape-morphing through folding or unfolding creases and limited local actuation in functionally identified graded origami architectures. In the following paragraphs, we will briefly review the progress in origami-assisted shape-morphing and the prospects of achieving target curvatures.

Origami spring-inspired shape morphing and its application in soft robotics is investigated by Chen et al. [35], wherein the nonlinear stretch-twist coupling of the springs has been considered. Cui et al. combined two approaches to produce composite sheets by embedding a stiff origami/kirigami skeleton with creases into thermal shrinkable polymer sheets for constructing innovative three-dimensional structures with curved surfaces from flat sheets [36]. Xu et al. proposed a flexible arc-armor inspired by origami, similar to the traditional fish-scale armor assembly form [37]. Xiang et al. investigated the energy absorption capability of origami-inspired structures with different straight and curved profiles [38]. Mukhopadhyay et al. proposed a waterbomb-based tubular origami for obtaining a range of convex, concave and programmable undulated shapes [39]. Further, Zhao et al. reported computational design

methods for cylindrical and axisymmetric waterbomb tessellations, leading to a range of target curved surfaces [40]. Zhang et al. proposed to exploit origami-based metasurfaces for designing stealth and radar technologies [41]. Meeussen and van Hecke developed multistable sheets with rewritable patterns for switchable shape-morphing [42], wherein they focus on undulating metasheets that store memories of mechanical stimuli in patterns of self-stabilizing scars. For achieving shape morphing, a significant number of studies have proposed kirigami patterns where cuts are introduced in addition to folding [43, 44]. Asma et al. reported curved-crease origami for a new class of morphing metamaterials [45]. Wang et al. developed inflatable metamorphic origami patterns with the advantage of being a highly simplified deployable system and capable of realizing multiple sequential motion patterns with a monolithic actuation [46]. Liu et al. developed robotic surfaces with reversible and spatiotemporal control for shape morphing and object manipulation [47]. Shape morphing and folding to curved surfaces have been proposed through generalized design methods and mechanics of Miura-based origami structures [48, 49], including multi-material 4D printing and embedded actuation [50, 51]. The brief literature review presented above reveals that while various other origami base patterns have been exploited for achieving target shapes and curvatures, adoption of Miura-ori architectures are rather limited despite their advantageous one degree of freedom kinematics. In the following section, we focus on the recent studies concerning Miura-based origami architectures, and subsequently, the aim and scope of this paper will be discussed.

Rigid origami is a subcategory of origami architectures that allows continuous mobility between folded states without the facets being twisted or stretched [52]. The miura base pattern is an elegant example of rigid origami with a single degree of freedom, which finds widespread application in the fields of engineering [53, 54]. The Miura-ori pattern is comprised of parallelogram facets that are identical to one another and surround the vertices of degree 4. Miura is an excellent choice for the design of foldable or deployable structures due to the fact that it possesses a high degree of symmetry, which is demonstrated by the fact that it has periodicity (in its conventional form), as well as four essential geometric features: (1) it is rigidly foldable, (2) it has only one degree of freedom, which determines the shape of the entire structure, (3) it possesses negative Poisson's ratio and (4) it is flat foldable [55]. Conventional Miura forms exhibit tessellation property, employing a repetitive unit cell geometry built from repeating a single tile size [56]. Miura-based patterns have recently been utilized in a variety of applications, including deployable folded plate shelters and curved canopy designs [57–60], subsea pipelines [61], automobile crash boxes [62], foldable reconfigurable reflect array antenna designs [63], and crawling robots [64]. Several different forms of rigid folding based on the Miura pattern have been reported in the literature including multi-layer and tubular architectures [65–67]. Constrained optimization algorithms have been

used to build rigid generalized Miura origami tessellations that can lead to curved surfaces with single or double curvature [68, 69]. A novel design of cylindrical and axisymmetric origami structures has been proposed based on generalized Miura-Ori cells, wherein the structure can fit between two given surfaces [70]. The coupling of layered Miura-origami architectures and rhombic honeycombs has been investigated to develop origami metamaterials with programmable two-stage compressive strength [71]. Further, Miura-ori pattern has been coupled with hexagonal honeycombs to develop 3D metamaterials with multi-directional Poisson's ratio modulation capabilities [72]. Miura-ori tesselations have been reported to be very effective in energy absorption, including as a core of sandwich structures [73]. Fang et al. performed a comprehensive experimental and analytical study on the dynamics of origami folding by investigating stacked Miura-Ori structures with intrinsic bistability, wherein both intrawell and interwell oscillations can be observed under harmonic base excitation [74]. Gattas and You presented the concept of curved creases in Miura-ori patterns along with their parametrization for a wide range of rigid-foldable applications [75]. Liu et al. proposed 4D Miura-based origami structures using shape memory alloys wherein a temperature-dependent programmable feature can be obtained [76]. The vast possibility of developing derivatives and piece-wise geometries concerning Miura-ori patterns has been investigated by altering a single characteristic of the Miura pattern among the identified five characteristics, crease orientation, crease alignment, developability, flat-foldability, and rectilinearity [77]. Such first-level derivatives lead to stiff foldable patterns with a wider variety of surface geometries, including non-zero values for both single and double curvature [60, 77, 78]. The capabilities of first-order Miura derivatives create a strong rationale for extending the parametrization to second-order derivatives with further expansion in the design space concerning two and three-dimensional shape morphing. This can be achieved by altering two or more parameters in the unit cell geometry and introducing spatial gradation in the origami structure. In the current paper, we will concentrate on such second-order graded derivatives of Miura-ori architectures (refer to Figure 1) based on detailed kinematic analyses and tabletop experiments.

Kinematic analysis of the Miura origami models has received significant attention given that it is a type of rigid origami which finds widespread engineering applications. The field of kinematics focuses on mechanisms and motion geometry, eliminating any consideration of the forces operating on the mechanism [79, 80]. When observed from the standpoint of a mechanism, the creases of origami can be interpreted as rotation joints, while the facets can be interpreted as links [81]. Spherical linkages are often used for analyzing Miura-ori folding mechanics, wherein it is characterized by a pattern consisting of a single vertex and having all creases intersect at the vertex [82]. The rigid foldability of a pattern with many vertex creases can be assessed using kinematic approaches where the pattern is viewed as a network of

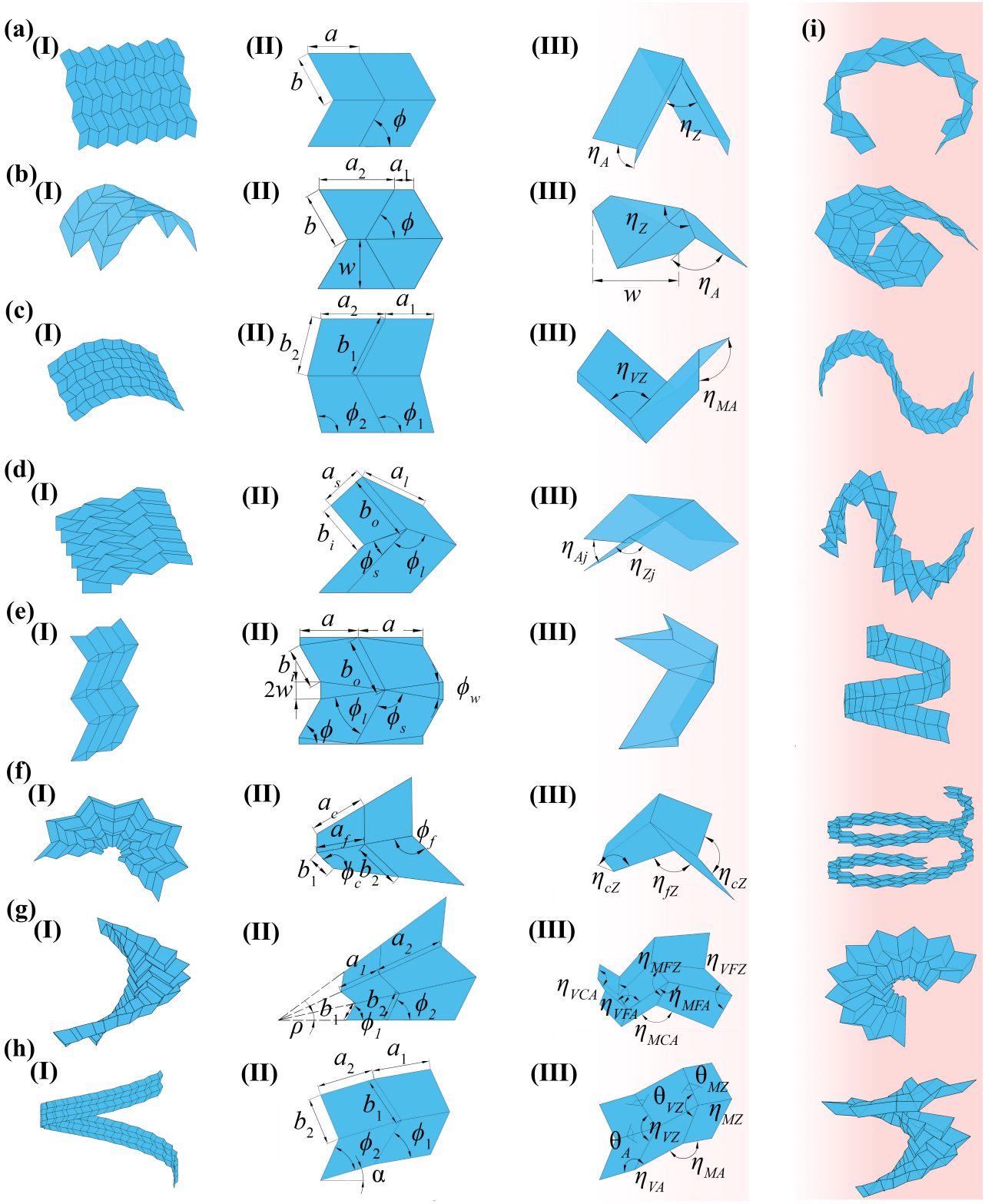

Figure 1: Geometrical architecture of Miura origami and its derivatives. For each of the Miura bases in subfigures (a-h), we show the tessellated architecture (first column), unit cell dimensions (second column), and partially folded state of the unit cells (third column). **(a)** Conventional Miura origami and its planar deployment. The subsequent origami unit cells are obtained by modifying the conventional Miura geometry. **(b)** Arc pattern with reverse crease orientation **(c)** Arc Miura origami with modified crease alignment **(d)** Non-developable Miura pattern with modified developability characteristics **(e)** Non-flat foldable Miura pattern with modified flat-foldability characteristics **(f)** Tapered Miura origami with modified rectilinearity characteristics **(g)** Tapered Arc Miura origami obtained by coupling of tapered Miura and Arc Miura origami **(h)** Inclined Arc Miura origami obtained by inclining straight creases of Arc Miura origami **(i)** A typical representation of the symmetric and asymmetric curvatures achieved through the Miura derivatives.

spherical links [83–85]. The kinematic analysis has been widely used to study and understand the motion behavior of origami patterns, leading to a mapping among the independent degrees of freedom and the deformed shape of the structure at any particular instance of the deformation [86, 87].

The conventional Miura pattern leads to in-plane deformation without any three dimensional shape morphing. We would propose derivatives of the Miura geometry by strategic modifications in the unit cell that lead to achieving target curvatures, wherein the asymmetry can further be controlled through geometric gradations. In the current study, we will focus on developing the kinematic relations for a range of second-order graded derivatives of the Miura-ori architectures considering symmetric and asymmetric geometries, leading to target curvatures through two to three-dimensional state transitions. The outcomes of the kinematic analyses will further be validated and supported by creating physical prototypes. Through the proposed second-order graded derivatives like Arc Miura, inclined Arc Miura, and tapered Arc Miura, we will demonstrate real-time programmable mechanical features including shape morphing ability in metamaterials and metasurfaces along with state-transitional deployment which can be crucial for a range of advanced engineering applications across the length scales.

2. Kinematic mapping of the motion behavior

2.1. Miura-ori architecture and its higher order derivatives

Miura-ori origami is a rigid origami architecture that has been extensively adopted in engineering applications due to its unprecedented properties such as negative Poisson's ratio, single degree of freedom, rigid foldability, flat foldability, and developability. The Miura base pattern is formed from four identical parallelogram plates (refer to Figure 1(a)). First- or second-order derivatives are produced when one or more of the Miura base pattern's features are altered. First-order derivative base patterns such as Arc pattern and Arc-Miura (Figure 1(b,c)), non-developable Miura (Figure 1(d)), non-flat foldable Miura (Figure 1(e)), and tapered Miura (Figure 1(f)) are developed by changing features like crease orientation and crease alignment, developability, flat-foldability, and rectilinearity, respectively. When the features of the first-order derivatives are further modified, second-order derivatives emerge. The second-order derivatives can also be obtained by introducing spatial gradation while assembling the unit cells of first-order derivatives for forming the tessellations. The repetition of these first or second-order derivatives can result in the formation of curved profiles, which is the central theme of this paper.

In the following sections, we will demonstrate that the first-order derivative leads to the formation of unidirectional curves and S-curves. However, these first-order derivatives are not enough to achieve helical curves of different kinds. To achieve these curves, we need to modify the first-order derivatives, resulting in the formation of second-order derivatives such as tapered Arc Miura pattern (Figure 1(g)) and inclined

Arc Miura pattern (Figure 1(h)). The attainment of unidirectional, S and helical (with orthogonal and planar rims) curves are discussed in adequate detail in the following sections along with the respective kinematic analysis framework. These curves are generally symmetric in nature when no spatial variation in the geometric features are considered. To achieve target asymmetry in these 3D curvatures, we would further incorporate spatial gradation in the Miura geometry. Gradation is the process of altering one or more independent variables in order to obtain a distinct symmetric and asymmetric curvature. In the next subsection, we will focus on the parametrization and kinematic mapping for first and second-order derivatives of Miura-ori including spatial gradation to achieve symmetric and asymmetric curvatures along with two to three-dimensional state transition. Our specific focus will be on the kinematics of Arc Miura, inclined Arc Miura and tapered Arc Miura architectures for achieving the target curvatures in three dimensions using developable origami folding.

2.2. Kinematic analysis of unit cell geometry

Kinematic analysis on the foldability and motion behavior of the tessellations that are formed from the four-crease Arc Miura, inclined Arc Miura and tapered Arc Miura bases is presented here. The folding of zero-thickness bases can be modeled kinematically as spherical 4R linkage. This unit linkage has one mountain crease and three valley creases. Given a $\beta_{i(i+1)}$ angle of rotation, the relationship between different dihedral angle (ϕ) as a function of the β can be derived as (refer to the supplementary material section S1 and Figures S3, S4, for detailed derivation and validation).

$$\frac{\tan\frac{\phi_1}{2}}{\tan\frac{\phi_2}{2}} = \frac{\cos\frac{\beta_{23}+\beta_{12}}{2}}{\cos\frac{\beta_{23}-\beta_{12}}{2}} \tag{1a}$$

$$\frac{\tan\frac{\phi_2}{2}}{\tan\frac{\phi_3}{2}} = \frac{\cos\frac{\beta_{23}-\beta_{12}}{2}}{\cos\frac{\beta_{23}+\beta_{12}}{2}} \tag{1b}$$

$$\frac{\tan\frac{\phi_3}{2}}{\tan\frac{\phi_4}{2}} = \frac{\cos\frac{\beta_{23}+\beta_{12}}{2}}{\cos\frac{\beta_{23}-\beta_{12}}{2}} \tag{1c}$$

$$\frac{\tan\frac{\phi_4}{2}}{\tan\frac{\phi_1}{2}} = \frac{\cos\frac{\beta_{23}-\beta_{12}}{2}}{\cos\frac{\beta_{23}+\beta_{12}}{2}} \tag{1d}$$

In the following paragraphs, we discuss the motion behavior of three different first and second-order derivatives of Miura origami architectures.

Kinematic motion behavior of Arc Miura pattern. Arc Miura pattern is a first-level derivative of the Miura origami, created by modifying the crease alignment characteristics of the Miura base pattern (refer to Figure 1(c)). Arc Miura folded configuration consists of m straight lines and n zigzag lines where i' varies from 1, 2, ..., m straight lines and j' varies from 1, 2, ..., n zigzag lines. i' denotes the number of straight creases and j' denotes the number of zigzag crease. Its coordinates at a vertex $K_{i',\,j'}$ can be

found out by 3D cylindrical coordinates where $(x,\, y,\, z) = (r\cos\theta,\, y,\, r\sin\theta)$ with respect to origin. The term origin in this context refers to the initial coordinates of vertex $K_{i',\, j'}$, which are located at (0, 0, 0). The components $(r,\, \theta,\, y)$ are given as

$$r = \begin{cases} R_1 & \text{for odd } j' \\ R_2 & \text{for even } j' \end{cases} \tag{2}$$

$$\theta = \begin{cases} (j'-1)\frac{\zeta}{2} & \text{for odd } i' \text{ and odd } j' \\ (j'-1)\frac{\zeta}{2} + \zeta_{b1} & \text{for even } i' \text{ and odd } j' \\ (j'-2)\frac{\zeta}{2} + \zeta - \zeta_{a2} & \text{for odd } i' \text{ and even } j' \\ (j'-2)\frac{\zeta}{2} + \zeta_{b1} + \zeta_{a2} & \text{for even } i' \text{ and even } j' \end{cases} \tag{3}$$

$$y = (i'-1)b_1 \sin\frac{\eta_{MZ}}{2} \tag{4}$$

The variable r, ζ, ζ_{a2} and ζ_{b1} are given in supplementary material section S2. 3D coordinates are used to achieve unidirectional and S curvature.

Kinematic motion behavior of inclined Arc Miura pattern. Inclined Arc Miura is a modified version of Arc Miura that is formed by inclining all the straight creases of Arc Miura at an angle α (refer to Figure 1(c, h) for Arc Miura and inclined Arc Miura patterns). Inclined Arc Miura folded configuration consists of m straight lines and n zigzag lines where i' varies from $1,\ 2, \ldots m$ straight lines and j' varies from $1,\ 2, \ldots n$ zigzag lines. i' denotes the number of straight creases and j' denotes the number of zigzag crease. Location of any vertex $K_{i',\, j'}$ can be found out by 3D cylindrical coordinates where $(x,\, y,\, z) = (r\cos\theta,\, y,\, r\sin\theta)$ with respect to origin. The term origin in this context refers to the initial coordinates of vertex $K_{i',\, j'}$, which are located at (0, 0, 0). The components $(r,\, \theta,\, y)$ are given as

$$r = \begin{cases} R_1 & \text{for odd } j' \\ R_2 & \text{for even} j' \end{cases} \tag{5}$$

$$y = \begin{cases} (i'-1)b_1 \sin\frac{\eta_{MZ}}{2} + \frac{j'-1}{2}a_2 \sin\alpha + a_1 \sin\alpha & \text{for odd } i' \text{ and odd } j' \\ (i'-1)b_1 \sin\frac{\eta_{MZ}}{2} + \frac{j'-1}{2}a_2 \sin\alpha + a_1 \sin\alpha & \text{for even } i' \text{ and odd } j' \\ (i'-1)b_1 \sin\frac{\eta_{MZ}}{2} + \frac{j'}{2}a_1 \sin\alpha + (\frac{j'}{2}-1)a_2 \sin\alpha & \text{for odd } i' \text{ and even } j' \\ (i'-1)b_1 \sin\frac{\eta_{MZ}}{2} + \frac{j'}{2}a_2 \sin\alpha + (\frac{j'}{2}-1)a_1 \sin\alpha & \text{for even } i' \text{ and even } j' \end{cases} \tag{6}$$

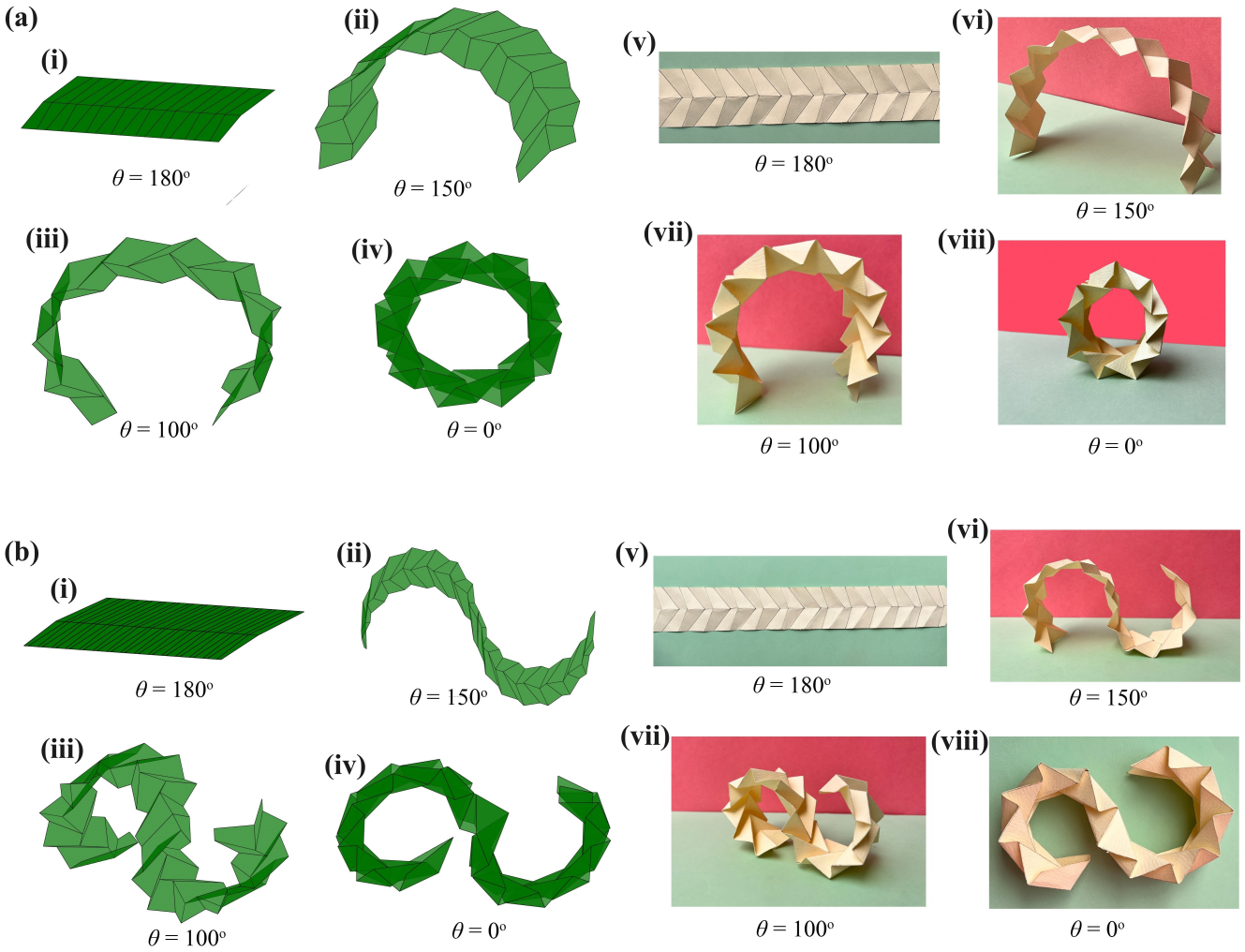

Figure 2: Programmable uni- and bi-directional shape morphing with symmetric architectures. **(a)** Programmable unidirectional curvature formed from Arc Miura assemblies and qualitative validation using physical prototypes. **(i - iv)** Unfolded flat, partially-, and fully-foldable configurations of unidirectional curvature at a dihedral angle $(\theta) = 180^o$, 150^o, 100^o, 0^o respectively. **(v - viii)** Physical prototypes corresponding to the computationally obtained programmable unidirectional curvatures. Note that the obtained curvatures are symmetric about the mid-length. **(b)** Programmable bidirectional S-shaped curvature formed from Arc Miura assemblies and qualitative validation using physical prototypes. **(i - iv)** Unfolded flat, partially-, and fully-foldable configurations of bidirectional curvature at a dihedral angle $(\theta) = 180^o$, 150^o, 100^o, 0^o respectively. **(v - viii)** Physical prototypes corresponding to the computationally obtained programmable bidirectional curvatures. Note that the obtained curvatures are symmetric (more precisely, anti-symmetric) about the mid-length. Note: θ denotes the dihedral angle, i.e., the angle formed between the two panels along a crease.

$$\theta = \begin{cases} (j'-1)\frac{\zeta}{2} & \text{for odd } i' \text{ and odd } j' \\ (j'-1)\frac{\zeta}{2} + \zeta_{b1} & \text{for even } i' \text{ and odd } j' \\ (j'-2)\frac{\zeta}{2} + \zeta - \zeta_{a2} & \text{for odd } i' \text{ and even } j' \\ (j'-2)\frac{\zeta}{2} + \zeta_{b1} + \zeta_{a2} & \text{for even } i' \text{ and even } j' \end{cases} \tag{7}$$

The variable r, ζ, ζ_{a2}, ζ_{b1} and η_{MZ} are given in supplementary material section S2. 3D coordinates are used to achieve helical curvature.

Kinematic motion behavior of tapered Arc Miura pattern. The tapered Arc Miura pattern is obtained

by coupling the tapered Miura pattern and Arc Miura pattern in order to enable both in-plane and out-of-plane deployment features (refer to Figure 1(c, f, g) for Arc Miura, tapered Miura and tapered Arc Miura patterns). An Arc Miura pattern can be converted into a tapered Arc Miura pattern by tilting the straight crease lines in the Arc Miura pattern. Tapered Arc Miura folded configuration consists of m straight lines and n zigzag lines where i' varies from 1, 2, ... m straight lines and j' varies from 1, 2, ... n zigzag lines. i' denotes the number of straight creases and j' denotes the number of zigzag crease. Location of any vertex $K_{i',\,j'}$ can be found out by 3D cylindrical co-ordinates where $(x,\, y,\, z) = (r\cos\theta,\, r\sin\theta,\, z)$ with respect to origin. The term origin in this context refers to the initial coordinates of vertex $K_{i',\,j'}$, which are located at (0, 0, 0). The components $(r,\, \theta,\, z)$ are given as

$$r = \begin{cases} R_C & \text{for odd } i' \\ R_F & \text{for even } i' \end{cases} \tag{8}$$

$$\theta = (i' - 1)\ \zeta \tag{9}$$

$$z = \begin{cases} \frac{(i'+1)}{2} a_1 \cos\frac{\eta_{MCA}}{2} & \text{for odd } j' \\ \frac{(i'-2)}{2} a_1 \cos\frac{\eta_{MCA}}{2} & \text{for even } j' \end{cases} \tag{10}$$

The variable r, ζ, and η_{MCA} are given in supplementary material section S2. 3D coordinates are used to achieve tapered Arc Miura piecewise geometries.

2.3. Kinematics of tessellated architectures

In the following section, we demonstrate a programmable attainment of curvature which can be achieved by varying the dihedral angle. In general, dihedral angles are formed by the adjacent faces of an origami fold and are preferred in origami research to directly represent the folding process. The piecewise assembling of the Arc Miura sequences (with or without gradations) results in variable rigid foldable symmetric and asymmetric curves. In the piecewise assembly algorithm, the parameters of the initial Miura units are provided, and the subsequent Miura unit is attached to the initial Miura unit on common edge vertices, therefore limiting the number of independent parameters. The initial Miura unit is known as the main pattern (m), and the followed Arc Miura unit is known as the slave pattern (s). By ensuring the continuity of the subsequent units in a tessellation (uniform or graded), symmetric and asymmetric continuous curvatures are obtained, as discussed in the following section.

3. Results and discussion

In this section, we will systematically demonstrate the attainment of programmable curvatures based on the kinematic motion behavior and experiments using physical prototypes. It can be noted in this context that a single Miura origami architecture is capable of assuming different degrees of curvature depending on the actuation provided by a single degree of freedom, leading to the notion of active and on-demand programmability.

3.1. Programmable asymmetry in unidirectional curvatures

Programmable symmetric and asymmetric unidirectional curvatures are realized here through uniform and graded Arc Miura architectures, respectively. In unidirectional Arc Miura tessellation redundant parameters are $b_1^m = b_1^s$, $\phi_1^m = \phi_1^s$, $m^m = m^s$ and folding variable $\theta_{MZ}^m = \theta_{MZ}^s$ where, b_1 is the side length, m is the number of straight lines, ϕ_1 is the sector angle and θ_{MZ} is the longitudinal dihedral angle at M-vertices (refer to Figure 1(c)). The configurations shown in Figure 2(a) are formed using the following parameters: n (number of zigzag lines) = 30, m (number of straight lines) = 3, a_1 = 30 mm, b_1 = 30 mm, L (total length of unit cell) = 90 mm, sector angles $\phi_1 = 60^o$ and $\phi_2 = 40^o$ and θ varied from 180^o to 0^o. The unidirectional curve assumes a completely unfolded configuration resembling a flat sheet at a dihedral angle $(\theta) = 180^o$ (refer to Figure 2(a(i))). With the decrease of dihedral angle $(\theta) = 150^o$, as depicted in Figure 2(a(ii)), the assembly achieves a partially-folded configuration resembling a parabola. With a further decrease in the dihedral angle $(\theta) = 100^o$, as depicted in Figure 2(a(iii)), the parabolic configuration becomes more compact. When the dihedral angle (θ) reaches 0^o, the configuration is fully folded and takes on a circular shape due to the full folding of creases (refer to Figure 2(a(iv))). The curvature programming from unfolded to fully folded configuration is validated using a physical prototype shown in Figure 2(a(v)-a(viii)), wherein an excellent agreement is observed with the motion simulation results.

A programmable unidirectional curvature, as shown in the Figure 2(a), provides symmetric curvature, while spatially varying and asymmetric curvature can be achieved through designed parametric gradation. Gradation involves the process of altering independent geometric variables to obtain distinct (i.e. target) symmetric and asymmetric curvatures. In the current investigation, to introduce gradation we have varied the sector angle ϕ_2 (following predefined gradation rules and geometric parametrizations) at each unit cell geometry while keeping all other independent variables constant. Figure 3 demonstrates the attainable symmetric and asymmetric curvatures of the unidirectional curves through gradation. The unidirectional curvature variation shown in the Figure 3(a) can be obtained by varying the sector angle ϕ_2 according to $\phi_2 = \phi_2 + s\delta\phi_2$ geometric parametrization, where ϕ_2 is the initial sector angle, s is number of unit

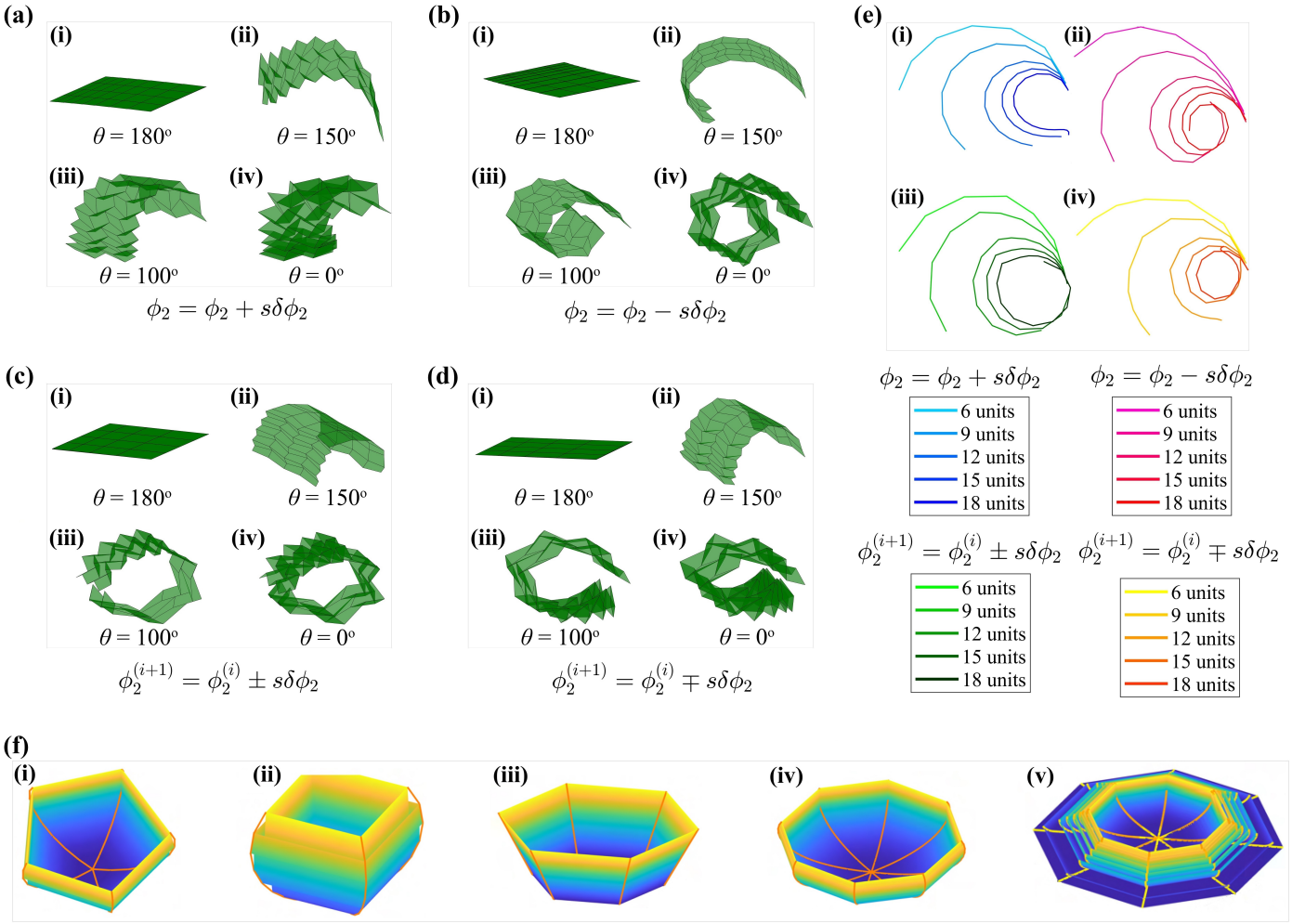

Figure 3: Programmable asymmetric unidirectional curvatures obtained through graded Miura derivatives. For achieving a target asymmetry in the unidirectional curvatures, we introduce geometric gradation by varying the sector angle (ϕ_2) at every unit cell while keeping the other independent variables constant. **(a)** Gradation is provided using $\phi_2 = \phi_2 + s\delta\phi_2$ where $\phi_2 = 30^o$, s is the number of unit cell and $\delta\phi_2 = 2^o$ **(i - iv)** Origami configurations at dihedral angle (θ) = 180^o, 150^o, 100^o and 0^o respectively. **(b)** Gradation is provided using $\phi_2 = \phi_2 - s\delta\phi_2$ where $\phi_2 = 50^o$, s is the number of unit cell and $\delta\phi_2 = 2^o$ **(i - iv)** Origami configurations at dihedral angle (θ) = 180^o, 150^o, 100^o and 0^o respectively. **(c)** Gradation is provided for $i = 0$ to $\frac{n}{2}$ using $\phi_2^{(i+1)} = \phi_2^{(i)} + s\delta\phi_2$ and for $i = \frac{n}{2}$ to n using $\phi_2^{(i+1)} = \phi_2^{(i)} - s\delta\phi_2$ where n is number of zigzag crease line, $\phi_2^{(i)} = 40^o$, s is the number of unit cell and $\delta\phi_2 = 2^o$ **(i - iv)** Origami configurations at dihedral angle (θ) = 180^o, 150^o, 100^o and 0^o respectively. **(d)** Gradation is provided for $i = 0$ to $\frac{n}{2}$ using $\phi_2^{(i+1)} = \phi_2^{(i)} - s\delta\phi_2$ and for $i = \frac{n}{2}$ to n using $\phi_2^{(i+1)} = \phi_2^{(i)} + s\delta\phi_2$ where n is number of zigzag crease line, $\phi_2^{(i)} = 40^o$, s is the number of unit cell and $\delta\phi_2 = 2.5^o$ **(i - iv)** Origami configurations at dihedral angle (θ) = 180^o, 150^o, 100^o and 0^o respectively. **(e)** Variation of unidirectional curvature while keeping the total length of the origami tessellation the same and increasing the number of unit cells. The asymmetric curvatures are presented considering the gradation schemes of Figures (a - d). **(f) (i - iv)** Three-dimensional programmable metasurfaces of different shapes obtained using multiple symmetric origami ribs **(v)** Schematic representation of the deployment of a three-dimensional metasurface with programmable curvature. Note: θ denotes the dihedral angle, i.e., the angle formed between the two panels along a crease; ϕ_2 denotes the initial sector angle; s is the number of unit cell of the Arc Miura pattern; $\delta\phi_2$ is the step size to change the ϕ_2 value; and n denotes the number of zigzag crease lines.

geometry and $\delta\phi_2$ is the step size to change the ϕ_2 value. With the increase of the sector angle (ϕ_2) from one end of the curve to the other, the unidirectional curve (Figure 3(a)) corresponding to $\phi_2 = 30^o$ and $\delta\phi_2 = 2^o$ initially experiences an increase in curvature variation, followed by a diminishing curvature.

The unfolded, partially-folded and fully-folded configurations of this unidirectional curve are obtained at dihedral angles (θ) = 180^o, 150^o, 100^o and 0^o respectively shown in Figure 3(a(i)-a(iv)). When the sector angle (ϕ_2) is varied according to $\phi_2 = \phi_2 - s\delta\phi_2$ geometric parametrization, where $\phi_2 = 50^o$ and $\delta\phi_2 = 2^o$ in order to obtain the unidirectional curve (Figure 3(b)), it is noticed that the unidirectional curve leads to a spiral curvature as the sector angle (ϕ_2) decreases from one end to the other. The variation of dihedral angle (θ) from 180^o to 0^o results in inward folding of the unidirectional curve as shown in Figure 3(b(i)-b(iv)).

When the sector angle (ϕ_2) is varied according to $\phi_2^{(i+1)} = \phi_2^{(i)} \pm s\delta\phi_2$ geometric parametrization, then unidirectional curvatures with different degrees are obtained as shown in Figure 3(c). Note that we introduce the superscript i in this geometric parametrization representing the number of zigzag creases. When i is varied from 0 to $\frac{n}{2}$, gradation is provided according to $\phi_2 = \phi_2 + s\delta\phi_2$ and when i varied from $\frac{n}{2}$ to n, gradation is provided according to $\phi_2 = \phi_2 - s\delta\phi_2$. The unidirectional curve shown in Figure 3(c) is obtained corresponding to $\phi_2 = 40^o$, $\delta\phi_2 = 2^o$ and $n = 20$. The unidirectional curve initially forms more compact creases when the sector angle (ϕ_2) increases from $i = 0$ to $\frac{n}{2}$ (with gradually diminishing compactness towards the middle) and shows increasing compactness as sector angle (ϕ_2) decreases from $i = \frac{n}{2}$ to n. As the dihedral angle (θ) decreases from 180^o to 0^o, the unidirectional curvature transitions from a flat sheet (unfolded configuration) to a more accentuated symmetric curvature (fully-folded configuration), as depicted in Figure 3(c(i)-c(iv)).

When sector angle(ϕ_2) is varied according to $\phi_2^{(i+1)} = \phi_2^{(i)} \mp s\delta\phi_2$ geometric parametrization, then the unidirectional curvature is obtained as shown in Figure 3(d). In this geometric parametrization, when i is varied from 0 to $\frac{n}{2}$, the gradation is provided according to $\phi_2 = \phi_2 - s\delta\phi_2$, and when i is varied from $\frac{n}{2}$ to n, gradation is provided according to $\phi_2 = \phi_2 + s\delta\phi_2$. The unidirectional curvature shown in Figure 3(d) is obtained corresponding to $\phi_2 = 40^o$, $\delta\phi_2 = 2.5^o$ and $n = 20$. Here the unidirectional curve initially experiences less folding when the sector angle (ϕ_2) decreases from $i = 0$ to $\frac{n}{2}$ and shows less compactness as sector angle (ϕ_2) increases from $i = \frac{n}{2}$ to n. As the dihedral angle (θ) decreases from 180^o to 0^o, the unidirectional curvature changes from a flat sheet (unfolded configuration) to a symmetric curvature (fully-folded configuration), as depicted in Figure 3(d(i)-d(iv)). Interestingly, the degree of unidirectional curvature in this geometric parametrization is observed to be inverted when compared with the curvature of Figure 3(c).

We have further investigated the influence of varying the number of unit geometries on the curvature of a unidirectional metastructure (refer to Figure 3(e)) while keeping the total length of the configuration constant at 90 mm. The number of units we have considered are 6, 9, 12, 15, and 18 with the earlier

discussed geometric gradation parametrization (refer to the corresponding figure legends). It can be observed in Figure 3(e(i)) that for a greater number of units, the curves take a more accentuated form of asymmetric parabolic configuration. Figure 3(e(ii)) shows that when the number of units increases, the configuration of curves becomes more compact and forms a spiral shape. The configuration of the curve in Figure 3(e(iii)) becomes more accentuated and takes the shape of a close loop with the increases in number of units. Figure 3(e(iv)) depicts that as the number of units increases to 6 and 18, the configuration of the curve becomes more condensed as compared with Figure 3(e(iii)) and acquires the shape of a closed loop having a lesser diameter. In general, it can be noticed that with an increasing number of units, the curvature of the developable origami metastructure increases and the curve transitions from a wide, and less sharp to a narrow and sharper configuration with a target symmetric or asymmetric geometry.

3.2. Programmable bi-directional S curvatures with target asymmetry

A programmable modulation of the rigid foldable S-curve curvature is accomplished by varying the dihedral angles of Arc Miura architectures as demonstrated in Figure 2(b). The bi-directional curvature is achieved by combining the Arc Miura unit sequences in one half with the reverse crease alignment of Arc Miura unit sequences in the other half. In the Arc Miura base unit, the sector angle for M-vertices and V-vertices (i.e. mountain and valley vertices) are taken as ϕ_1 and ϕ_2 respectively, while in the reverse Arc Miura base unit, the sector angle for M-vertices and V-vertices are taken as ϕ_2 and ϕ_1 respectively. In the piecewise assembly, the parameters of the initial Arc Miura unit are provided, and the subsequent Arc Miura unit is attached to the initial Arc Miura unit on common edge vertices, therefore limiting the number of independent parameters. The initial Arc Miura unit is known as the main pattern (m), and the followed Arc Miura unit is known as the slave pattern (s). The redundant parameters are $b_1^m = b_1^s$, $\phi_1^m = \phi_1^s$, $m^m = m^s$ and folding variable $\theta_{MZ}^m = \theta_{MZ}^s$.

The configuration of S-curve shown in Figure 2(b) is formed using the following parameters: n (number of zigzag lines) = 30, m (number of straight lines) = 3, a_1 = 30 mm, b_1 = 30 mm, L (total length of unit cell) = 90 mm, sector angles $\phi_1 = 60^o$ and $\phi_2 = 40^o$, and θ in the range of 180^o to 0^o. The S curvature takes an unfolded configuration resembling the flat-folded sheet at a dihedral angle (θ) = 180^o (refer to Figure 2(b(i))). When the dihedral angle (θ) is reduced to 150^o, the curve achieves a partially-folded configuration showing bidirectional curvature, as depicted in Figure 2(b(ii)). With further decrease in the dihedral angle (θ) to 100^o, the curve shows a contracted bidirectional curvature resembling S shape (Figure 2(b(iii))). When the dihedral angle (θ) becomes 0^o, the curve achieves a fully-folded configuration resembling two near-zero thickness circles formed due to the complete folding of the creases (Figure 2(b(iv))). Physical demonstration of the programmable S curvature with different degrees from a flat

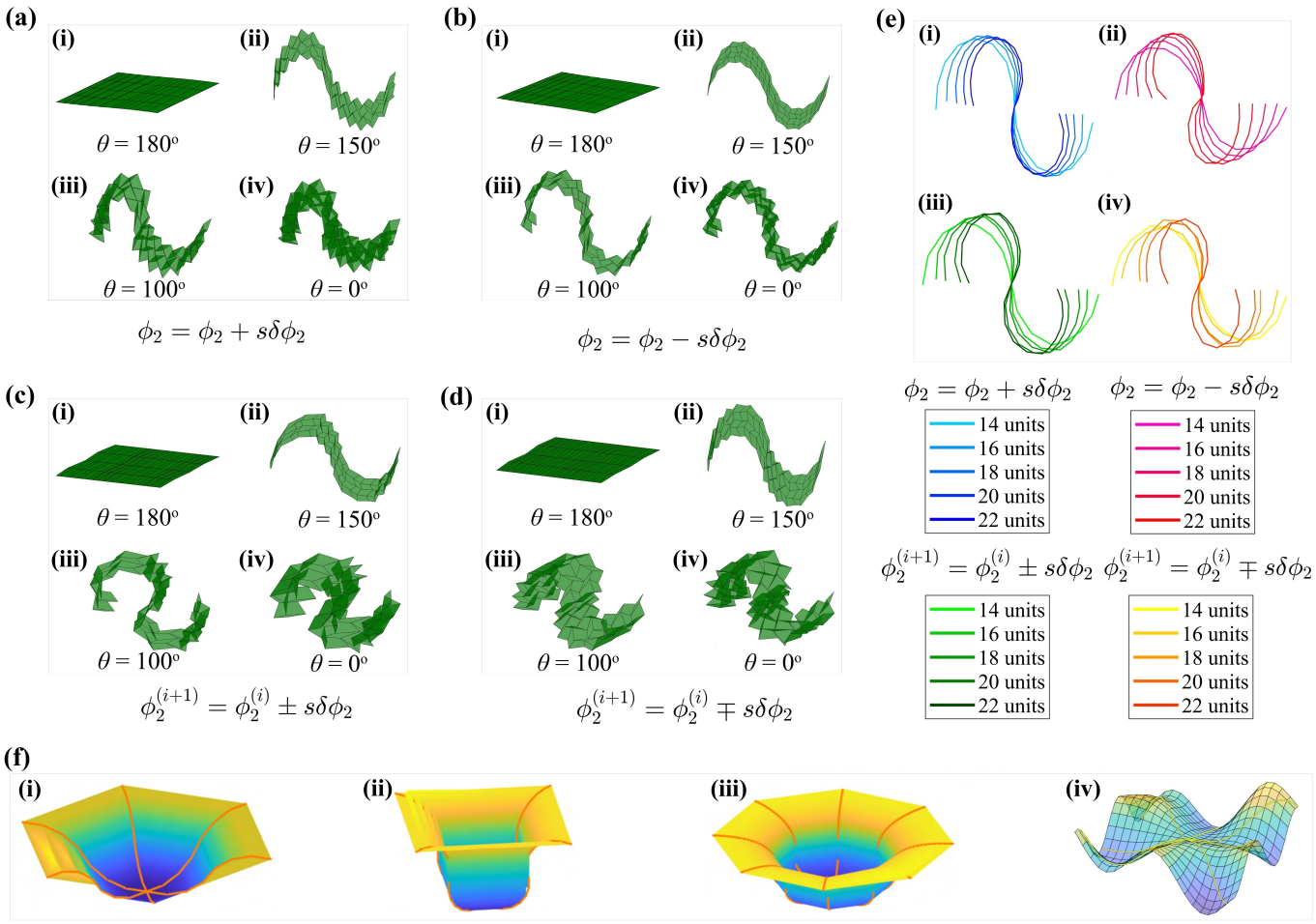

Figure 4: Programmable asymmetric S shape curvatures obtained through graded Miura derivatives. For achieving a target asymmetry in the unidirectional curvatures, we introduce geometric gradation by varying the sector angle (ϕ_2) at every unit cell while keeping the other independent variables constant. **(a)** Gradation is provided using $\phi_2 = \phi_2 + s\delta\phi_2$ where $\phi_2 = 30^o$, s is the number of unit cell and $\delta\phi_2 = 2^o$ **(i - iv)** Origami configurations at dihedral angle (θ) = 180^o, 150^o, 100^o, 0^o respectively. **(b)** Gradation is provided using $\phi_2 = \phi_2 - s\delta\phi_2$ where $\phi_2 = 50^o$, s is the number of unit cell and $\delta\phi_2 = 1^o$ **(i - iv)** Origami configurations at dihedral angle (θ) = 180^o, 150^o, 100^o, 0^o respectively. **(c)** Gradation is provided for $i = 0$ to $\frac{n}{2}$ using $\phi_2^{(i+1)} = \phi_2^{(i)} + s\delta\phi_2$ and for $i = \frac{n}{2}$ to n using $\phi_2^{(i+1)} = \phi_2^{(i)} - s\delta\phi_2$ where n is number of zigzag crease line, $\phi_2^{(i)} = 40^o$, s is the number of unit cell and $\delta\phi_2 = 2^o$ **(i - iv)** Origami configurations at dihedral angle (θ) = 180^o, 150^o, 100^o, 0^o respectively. **(d)** Gradation is provided for $i = 0$ to $\frac{n}{2}$ using $\phi_2^{(i+1)} = \phi_2^{(i)} - s\delta\phi_2$ and for $i = \frac{n}{2}$ to n using $\phi_2^{(i+1)} = \phi_2^{(i)} + s\delta\phi_2$ where n is number of zigzag crease line, $\phi_2^{(i)} = 40^o$, s is the number of unit cell and $\delta\phi_2 = 2^o$ **(i - iv)** Origami configurations at dihedral angle (θ) = 180^o, 150^o, 100^o, 0^o respectively. **(e)** Variation of bidirectional curvature while keeping the total length of the origami tessellation the same and increasing the number of unit cells. The asymmetric curvatures are presented considering the gradation schemes of Figures (a - d). **(f) (i - iii)** Three-dimensional programmable metasurfaces of different shapes with bi-directional curvature obtained using multiple bi-directional S-shaped origami ribs **(iv)** Schematic representation of a generic metasurface that can be obtained using optimally graded origami ribs using inverse design. Note: θ denotes the dihedral angle, i.e., the angle formed between the two panels along a crease; ϕ_2 denotes the initial sector angle; s is the number of unit cells of the Arc Miura pattern; $\delta\phi_2$ is the step size to change the ϕ_2 value; and n denotes the number of zigzag crease lines.

sheet to a completely compacted stage under the variation of dihedral angle from 180^o to 0^o is depicted in Figure 2(b(v)-b(viii))).

The symmetrical bi-directional S curvatures can be transformed into asymmetrical S curvatures through the incorporation of geometric gradation. The gradation is introduced by altering the sector

angle (ϕ_2) following different parametrization schemes at each unit geometry while keeping the other independent variables constant. The programmable S-curve depicted in Figure 4(a) is achieved by modifying the sector angle (ϕ_2) according to $\phi_2 = \phi_2 + s\delta\phi_2$ geometric gradation parametrization, where ϕ_2 is the initial sector angle, s is number of unit geometry and $\delta\phi_2$ is the step size to change the ϕ_2 value. The S-curve obtained here is generated considering $\phi_2 = 30^o$ and $\delta\phi_2 = 2^o$. It can be observed that with the variation of sector angle (ϕ_2) from one end to the other end through the above parametrization scheme, asymmetric curvature can be achieved with narrower curvature on the left and wider curve on the right end (refer to Figure 4(a)). The unfolded, partially-folded and fully-folded configurations at dihedral angles (θ) = 180^o, 150^o, 100^o and 0^o respectively are shown in Figure 4(a(i)-a(iv)), demonstrating the curvature programmability of a single origami architecture from a flat state to two and three-dimensional state transitions.

The programmable S curvature shown in Figure 4(b) is obtained based on the alteration of sector angle (ϕ_2) through $\phi_2 = \phi_2 - s\delta\phi_2$ geometric gradation parametrization with $\phi_2 = 50^o$ and $\delta\phi_2 = 1^o$. It can be noticed that with the variation of sector angle (ϕ_2) from one end to the other end through the above parametrization, the nature of asymmetry becomes reverse to the configuration presented in Figure 4(a). As the dihedral angle (θ) decreases from 180^o to 0^o, the S-curve goes from a flat sheet (unfolded configuration) to an asymmetric S curvature (fully-folded configuration) as depicted in Figure 4(b(i)-b(iv)).

The programmable S curvatures demonstrated in Figure 4(c) is achieved by tailoring the sector angle (ϕ_2) according to the $\phi_2^{(i+1)} = \phi_2^{(i)} \pm s\delta\phi_2$ geometric gradation parametrization with $\phi_2 = 40^o$ and $\delta\phi_2 = 2^o$ and $n = 30$. In this geometric parametrization, gradation is provided according to $\phi_2 = \phi_2 + s\delta\phi_2$ for i ranging from 0 to $\frac{n}{2}$ and according to $\phi_2 = \phi_2 - s\delta\phi_2$ for i ranging from $\frac{n}{2}$ to n, where n is the number of zigzag creases. In the partially folded form, it forms a circular shape on both the left and right sides, with different radii, resembling the shape of a seahorse. The folding behavior of the asymmetric S curvature with the variation of dihedral angle (θ) from 180^o to 0^o can be observed in Figure 4(c(i)-c(iv)).

The programmable S curvatures depicted in Figure 4(d) is obtained by grading the sector angle (ϕ_2) according to this $\phi_2^{(i+1)} = \phi_2^{(i)} \mp s\delta\phi_2$ geometric gradation parametrization with $\phi_2 = 40^o$, $\delta\phi_2 = 2^o$ and $n = 30$. In this gradation architecture, the variation of sector angle (ϕ_2) is considered as follows: for i from 0 to $\frac{n}{2}$ through $\phi_2 = \phi_2 - s\delta\phi_2$ and for i from $\frac{n}{2}$ to n through $\phi_2 = \phi_2 + s\delta\phi_2$. It can be observed from the configurations that depending on the value of the dihedral angle (θ) the asymmetry in the S curvature can be programmed with different degrees (refer to Figure 4(d(iii)-d(iv))).

We have further investigated the influence of varying the number of unit geometries on the S curvature

of a bidirectional metastructure (refer to Figure 4(e)) while keeping the total length of the configuration constant at 90 mm. The number of units we have considered are 14, 16, 18, 20 and 22 with the earlier discussed geometric gradation parametrization (refer to the corresponding figure legends). It can be observed in Figure 4(e) that for a greater number of units, the curves take a more accentuated form of asymmetric or anti-symmetric S configuration depending on the gradation architecture. In general, with an increasing number of units, the curvature of the developable origami metastructure increases and the curve transitions from a wide, and less sharp to a narrow and sharper configuration with a target curved geometry, wherein a two to three-dimensional shape transition can be realized.

The two-dimensional curvatures depicted in Figures 3(a-d) and 4(a-d) can further be extended to 3D metasurfaces with target curvatures as shown in Figures 3(f) and 4(f). Multiple two-dimensional origami architectures can be attached to each other as ribs, wherein the ribs are interconnected by thin and flexible materials of functional interest. Interestingly, the three dimensional surfaces can be tailored to have unidirectional or bi-directional curvatures and different peripheral shapes with symmetric and asymmetric geometries depending on the rib origami architectures, their number and orientations. On-demand programmability in the surface curvatures can be achieved through controlling the dihedral angles of the ribs through limited actuation as depicted in Figure 3(f(v)). In principle, through appropriate spatial gradation of the rib origami architectures, the bi-directional curvatures can further be extended to have multi-directional surface curvatures as shown in Figure 4(f(iv)).

3.3. Programmable helical curvatures with orthogonal rims

A programmable variation of the rigid foldable helical curvature is accomplished through piece-wise assembly of the inclined Arc Miura architecture, as demonstrated in Figure 5. As shown in Figures 5 and 6, it can be noticed that the class of helical architectures discussed in this subsection possesses the rims orthogonal to the plane on which the helix rests, i.e. the elevation direction is parallel to the plane of rims. In the piecewise assembling of these helical curves, the parameters of initial inclined Arc Miura unit are provided and the unit is attached to the subsequent inclined Arc Miura unit through common edge vertices, therefore limiting the number of independent parameters. The initial unit is known here as main pattern (m) and the subsequent inclined Arc Miura unit is known as slave pattern (s). The redundant parameters are $b_1^m = b_1^s$, $\phi_1^m = \phi_1^s$, $m^m = m^s$ and folding variable $\theta_{MZ}^m = \theta_{MZ}^s$. The configurations of helical curve shown in Figure 5 is achieved according to the following parameters: n (number of zigzag lines) = 40, m (number of straight lines) = 5, a_1 = 30 mm, b_1 = 30 mm, L (total length of unit cell) = 90 mm, sector angles $\phi_1 = 60^o$ and $\phi_2 = 40^o$, $\alpha = 12^o$ and θ is varied from 180^o to 0^o.

The helical curvature assumes a two-dimensional flat sheet shape (unfolded configuration) at a dihedral

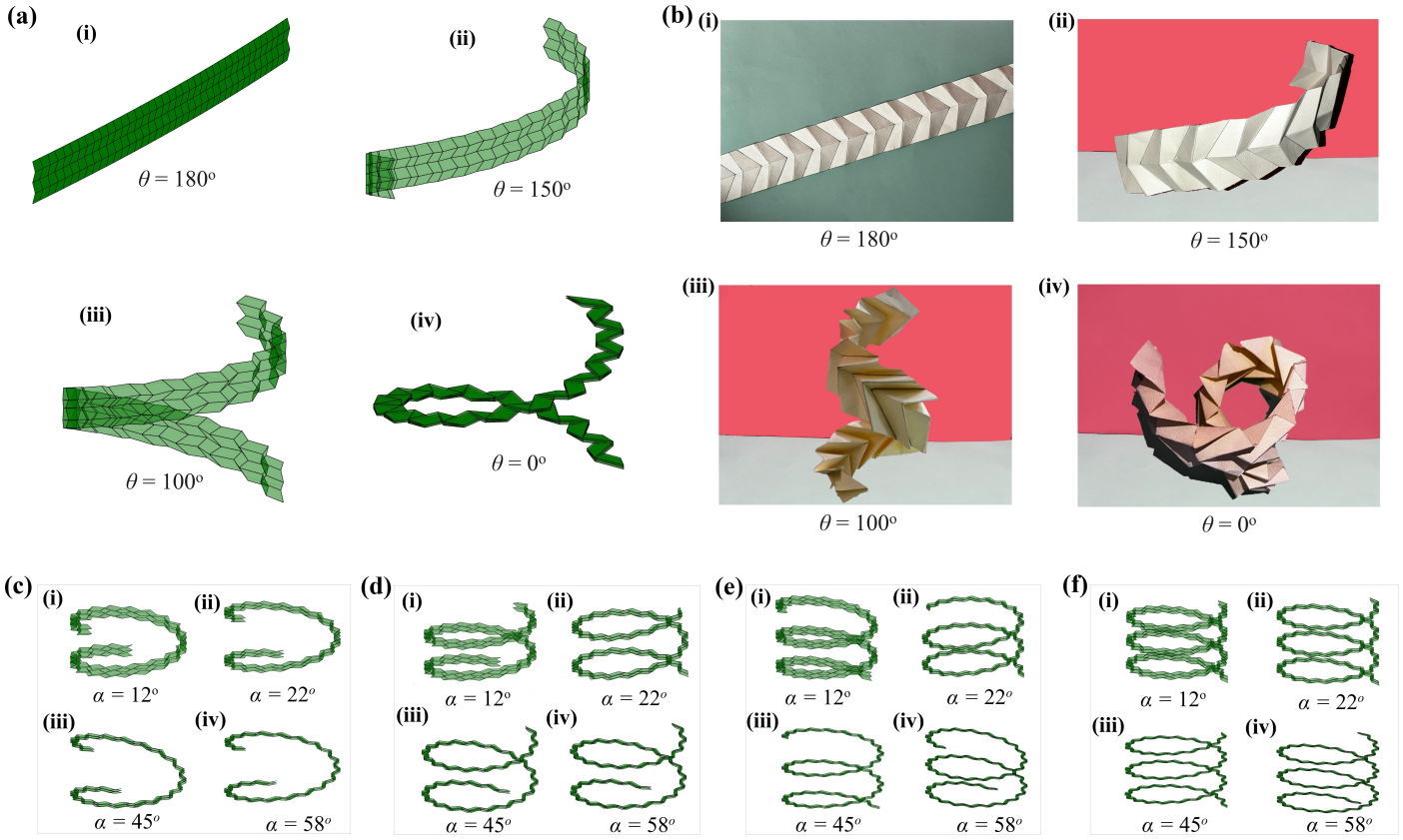

Figure 5: Programmable helical curvatures with elevation-wise uniform geometry and orthogonal rims. (a) Programmable helical curvature formed using inclined Arc Miura assemblies. **(i - iv)** Unfolded flat-, partially-, and fully-folded configurations of helical curvature at a dihedral angle (θ) = 180^o, 150^o, 100^o, 0^o respectively **(b)** Physical prototype of helical curvature corresponding to the configurations shown in Figure (a) **(c)** Configuration of helical curvatures achieved by considering $n = 50$ with different values of α **(d)** Configuration of helical curvatures achieved by considering $n = 70$ with different values of α **(e)** Configuration of helical curvatures achieved by considering $n = 90$ with different values of α **(f)** Configuration of helical curvatures achieved by considering $n = 110$ with different values of α. Note: θ denotes the dihedral angle, i.e., the angle formed between the two panels along a crease; α denotes the inclination angle, i.e., the angle made by the straight edge of the inclined Arc Miura pattern with horizontal axes; n denotes the number of zigzag crease lines; and "pitch" denotes distance between successive turns of the helix.

angle (θ) = 180^o (refer to Figure 5(a(i))). As the dihedral angle (θ) is reduced to 150^o the helical curve demonstrates an elevation and starts folding in a helical form (Figure 5(a(ii))). With further decrease in the dihedral angle (θ) to 100^o, the elevation further increases, as depicted in Figure 5(a(iii)). When the dihedral angle (θ) reaches 0^o, the helical curve shows a fully compact folded helical shape as shown in Figure 5(a(iv)). The folding behaviour of the helical curve is validated through physical prototypes as illustrated in Figure 5(b(i)-b(iv)), wherein a perfect agreement can be observed with the computational motion analysis.

We have investigated the behaviour of the helical curvature with the variation in inclination angle (α) and number of zigzag lines (n) while maintaining the dihedral angle constant at $\theta = 120^o$. Here inclination angle is defined as the angle made by the straight edge of the inclined Arc Miura pattern with the horizontal axes (refer to supplementary material section S2.2). For the variation of zigzag line (n)

as 50, 70, 90 and 100, the inclination angle (α) is taken as 12^o, 22^o, 45^o and 58^o. When the number of zigzag line (n) is 50, the helical curve shows only one turn (Figure 5(c)). As the number of zigzag line (n) increases to 70, the helical curve shows two turns (Figure 5(d)). Further increasing the number of zigzag lines (n) to 110 results in the helical curve showing three turns (Figure 5(f)). It can be concluded that as the number of zigzag line (n) increases, the number of turns shown by the helical curve also increases. Additionally, the folding of the helical curve increases with the increase in inclination angle (α).

The programmable architecture of helical curves shown in Figure 5 will always result in symmetric uniform helical curvature. In order to achieve symmetric as well as asymmetric helical curvatures with elevation-wise varying diameter, we have further incorporated geometric gradation similar to the earlier subsections through the modification of sector angle (ϕ_2). The helical curvatures depicted in Figure 6(a) is achieved through the modification of sector angle (ϕ_2) according to $\phi_2 = \phi_2 + s\delta\phi_2$ geometric parametrization with $\phi_2 = 30^o$ and $\delta\phi_2 = 2^o$. The helical curve shows single turn, and the pitch of the helical curve increases with a decrease in the dihedral angle (θ). Moreover, the top end of the helical curve shows more contraction of inclined Arc Miura units due to the increasing value of sector angle (ϕ_2) as depicted in Figure 6(a(iii)-a(iv)).

The programmable helical curvatures in Figure 6(b) are obtained by the modification of sector angle (ϕ_2) according to this $\phi_2 = \phi_2 - s\delta\phi_2$ geometric parametrization with $\phi_2 = 50^o$ and $\delta\phi_2 = 1^o$. It can be noted that the helical curve displays two turns here depending on the assumed geometric parameters. Additionally, the diameter of the helical turns decreases as the curve starts taking the elevation. In Figure 6(b(iii)), it can be noticed that the pitch of the helical curve is nearly negligible at a dihedral angle (θ) of 100^o, but as the dihedral angle (θ) reduces to 0^o due to fully folding of the creases, the helical curve shows a significant pitch (Figure 6(b(iv))).

The curvatures in Figure 6(c) is achieved by the alteration of sector angle (ϕ_2) according to the $\phi_2^{(i+1)} = \phi_2^{(i)} \pm s\delta\phi_2$ geometric gradation parametrization with $\phi_2 = 40^o$, $\delta\phi_2 = 2^o$ and $n = 40$. The variation of i from 0 to $\frac{n}{2}$ provides the sector angle (ϕ_2) according to $\phi_2 = \phi_2 + s\delta\phi_2$ gradation scheme, while for the variation of i from $\frac{n}{2}$ to n provides the sector angle (ϕ_2) according to $\phi_2 = \phi_2 - s\delta\phi_2$ gradation scheme. The helical curve shows two turns, and the diameter of helical turns increases with an increase in the elevation as seen at dihedral angle (θ)= 0^o (Figure 6(c(iv))).

The programmable helical curve curvatures in Figure 6(d) is obtained by the tailoring of sector angle (ϕ_2) according to $\phi_2^{(i+1)} = \phi_2^{(i)} \mp s\delta\phi_2$ geometric parametrization with $\phi_2 = 40^o$, $\delta\phi_2 = 2^o$ and $n = 40$. The variation of i from 0 to $\frac{n}{2}$ provides the sector angle (ϕ_2) according to $\phi_2 = \phi_2 - s\delta\phi_2$ gradation scheme, while for the variation i from $\frac{n}{2}$ to n, provides the sector angle (ϕ_2) according to $\phi_2 = \phi_2 + s\delta\phi_2$

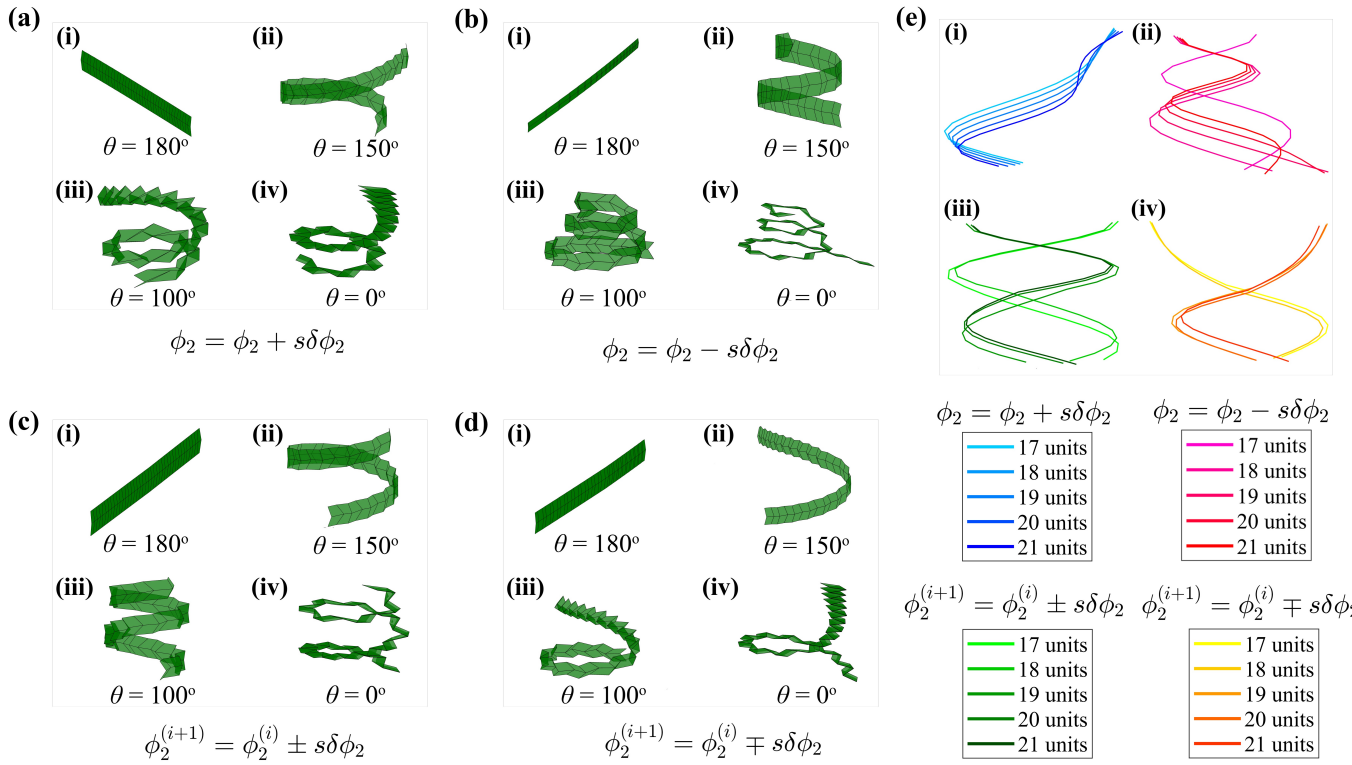

Figure 6: Programmable helical curvatures with elevation-wise varying geometric features and orthogonal rims. Geometric gradation is introduced by varying the sector angle (ϕ_2) at every unit cell and keeping the other independent parameters constant. **(a)** Gradation is provided using $\phi_2 = \phi_2 + s\delta\phi_2$ where $\phi_2 = 30^o$, s is the number of unit cell and $\delta\phi_2 = 2^o$ **(i - iv)** Origami configurations at dihedral angle (θ) = 180^o, 150^o, 100^o, 0^o respectively. **(b)** Gradation is provided using $\phi_2 = \phi_2 - s\delta\phi_2$ where $\phi_2 = 50^o$, s is the number of unit cell and $\delta\phi_2 = 1^o$. **(i - iv)** Origami configurations at dihedral angle (θ) = 180^o, 150^o, 100^o, 0^o respectively. **(c)** Gradation is provided for $i = 0$ to $\frac{n}{2}$ using $\phi_2^{(i+1)} = \phi_2^{(i)} + s\delta\phi_2$ and for $i = \frac{n}{2}$ to n using $\phi_2^{(i+1)} = \phi_2^{(i)} - s\delta\phi_2$ where n is number of zigzag crease line, $\phi_2^{(i)} = 40^o$, s is the number of unit cell and $\delta\phi_2 = 2^o$. **(i - iv)** Origami configurations at dihedral angle (θ) = 180^o, 150^o, 100^o, 0^o respectively. **(d)** Gradation is provided for $i = 0$ to $\frac{n}{2}$ using $\phi_2^{(i+1)} = \phi_2^{(i)} - s\delta\phi_2$ and for $i = \frac{n}{2}$ to n using $\phi_2^{(i+1)} = \phi_2^{(i)} + s\delta\phi_2$ where n is number of zigzag crease line, $\phi_2^{(i)} = 40^o$, s is the number of unit cell and $\delta\phi_2 = 2^o$. **(i - iv)** Origami configurations at dihedral angle (θ) = 180^o, 150^o, 100^o, and 0^o respectively. **(e)** Variation of helical curvature and asymmetry with increasing the number of unit cells while keeping the total length of the origami structure the same. The same gradation scheme as Figures (a - d) is utilized for this investigation. Note: θ denotes the dihedral angle, i.e., the angle formed between the two panels along a crease; ϕ_2 denotes the initial sector angle; s is the number of unit cells of the inclined Arc Miura pattern; $\delta\phi_2$ is the step size to change the ϕ_2 value; n denotes the number of zigzag crease lines; and "pitch" denotes distance between successive turns of the helix.

gradation scheme. The helical curve shows a single turn, and the crease at the top end of the helical curve is more contracted due to the increased sector angle (ϕ_2) (Figure 6(d(iv))). Furthermore, the helical curve completes full turns after fully folding the crease, which is only possible when the dihedral angle (θ) decreases from 180^o to 0^o.

We have further investigated the effect of changing the number of unit geometries on the curvature of a helical shape (Figure 6(e)) while keeping the total length of the configuration constant at 90 mm. The number of units we have considered are 17, 18, 19, 20 and 21, with the earlier discussed geometric gradation parametrization schemes. As depicted in Figure 6(e), the curvature of the helical architecture

gets more accentuated with symmetric or asymmetric variation along the curved profile as the number of units increases depending on the adopted gradation scheme. In general, the numerical results indicate that by adjusting the dihedral angle and incorporating gradation, it is possible to modify the pitch, diameter, and number of turns of a helical curve. Moreover, changing the number of geometric units along with gradation can also alter the orientation of the curve as per programmable demands. While the uniform architectures shown in Figure 5 result in uniform diameter along the elevation, the graded architectures presented in Figure 6 can lead to elevation-wise control in the diameter. The gradation schemes of Figure 6(a, b) show elevation-wise continuously decreasing or increasing diameter, and the gradation schemes of Figure 6(c, d) can achieve symmetric elevation-wise increasing or decreasing diameters about the mid-profile length. In this context, it may further be noted that the trend of elevation-wise diameter variation can be programmed in a more generic way to achieve target profiles by introducing appropriate gradation schemes following the proposed framework.

3.4. Programmable helical curvatures with planar rims

As discussed in the preceding subsection, it can be noticed that the helical architectures possess rims orthogonal to the plane on which the helix rests, i.e. the elevation direction is parallel to the plane of rims (refer to Figures 5 and 6). In this subsection, we propose a new class of second-order Miura origami resulting in circular and helical curvatures with planar rims (refer to Figure 7). It is worth further noting that all the unidirectional, bidirectional and helical curvatures investigated so far do not have in-plane rims (i.e. the plane of curvature and the plane of origami tessellation are not in the same plane), unlike the configurations we investigate here.

The helical curvatures with planar rims are obtained through piecewise assembling of tapered Arc Miura patterns with or without gradation, wherein the programmability is achieved by altering the dihedral angle, as depicted in Figure 7. In the piecewise assembly, the initial tapered Arc Miura unit (known as main pattern (m)) is attached to the subsequent similar tapered Arc Miura unit (known as slave pattern (s)). The parameters of main pattern is provided initially, and the attachment at the common vertex with the main pattern limits the number of independent parameters for the slave pattern. These redundant parameters are ${b_1}_j^m = {b_1}_{j+1}^s$, $\phi_1^m = \phi_1^s$, $(\phi_1 - \rho)^m = (\phi_1 - \rho)^s$, $m^m = m^s$ and folding variable $\theta_{MZ}^m = \theta_{MZ}^s$. The configurations of helical curves depicted in Figure 7 are generated using the following parameters: n (number of zigzag lines) = 5, m (number of straight lines) = 27, a_1 = 40 mm, b_1 = 20 mm, L (total length of unit cell) = 90 mm, sector angles $\phi_1 = 60^o$ and $\phi_2 = 50^o$, $\rho = 18^o$ and θ varied from 180^o to 90^o.

An unfolded configuration of the tapered Arc Miura assembly (flat sheet) at a dihedral angle (θ) = 180^o

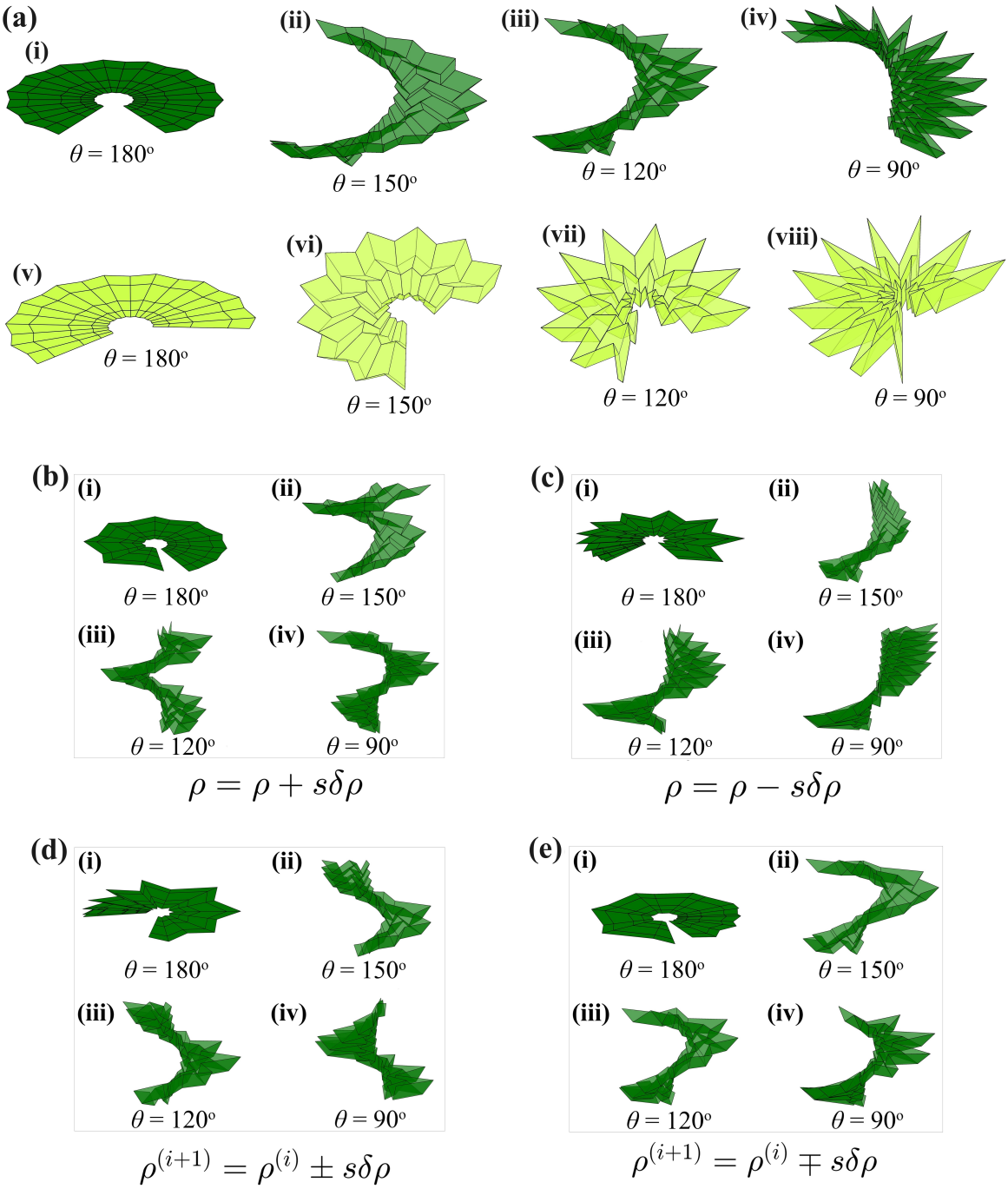

Figure 7: Programmable helical curvatures with elevation-wise varying geometric features and planar rims. **(a)** Programmable helical curvature formed from tapered Arc Miura assemblies. **(i - iv)** Unfolded flat-, partially- and fully-foldable configurations of helical curvatures at a dihedral angle $(\theta) = 180^o$, 150^o, 120^o, 90^o. **(v - viii)** A special case of circular deployment when both $\phi_1 = \phi_2$, and $\rho = 0$ conditions are satisfied **(b - e)** Origami configurations at dihedral angle $(\theta) = 180^o$, 150^o, 120^o, 90^o respectively considering different gradation schemes. (b) Gradation using $\rho = \rho + s\delta\rho$ where $\rho = 18^o$ and $\delta\rho = 1^o$. (c) Gradation using $\rho = \rho - s\delta\rho$ where $\rho = 28^o$ and $\delta\rho = 1^o$. (d) Gradation is provided for $i = 0$ to $\frac{m}{2}$ using $\rho^{(i+1)} = \rho^{(i)} + s\delta\rho$ and for $i = \frac{m}{2}$ to m using $\rho^{(i+1)} = \rho^{(i)} - s\delta\rho$ where $\rho^{(i)} = 25^o$ and $\delta\rho = 1.5^o$. (e) Gradation is provided for $i = 0$ to $\frac{m}{2}$ using $\rho^{(i+1)} = \rho^{(i)} - s\delta\rho$ and for $i = \frac{m}{2}$ to m using $\rho^{(i+1)} = \rho^{(i)} + s\delta\rho$ where $\rho^{(i)} = 28^o$ and $\delta\rho = 1.5^o$. Note: θ denotes the dihedral angle, i.e., the angle formed between the two panels along a crease; ρ denotes the angle between the straight crease lines; ϕ_1 and ϕ_2 denote the sector angles for adjacent zigzag creases with the straight crease; s is the number of unit cells of the tapered Arc Miura pattern; $\delta\rho$ is the step size to change the ρ value; m denotes the number of straight crease lines; and "pitch" denotes distance between successive turns of the helix.

is shown in Figure 7(a(i)). As the dihedral angle (θ) decreases to 150^o, the flat sheet takes a helical profile (Figure 7(a(ii))). With further decrease in dihedral angle (θ) to 120^o, the origami profile gets contracted due to the folding of creases (Figure 7(a(iii))). At a dihedral angle (θ) of 90^o, the configuration assumes the fully-folded helical profile as depicted in Figure 7(a(iv)). As a special case, when both $\phi_1 = \phi_2$, and $\rho = 0$ conditions are satisfied, the proposed architecture shows in-plane circular curvature with active programmability, as shown in Figure 7(a(v)-a(viii))). Similar in-plane circular curvatures have been presented in literature [77], which essentially improves the confidence in the current computational framework through qualitative validation.

Notably, the curvatures presented in Figure 7(a) do not have any spatial variation along the profile of the origami architecture. Symmetric and asymmetric curvatures can be achieved through the introduction of spatial geometric gradation, as demonstrated in Figure 7(b-e). The gradation is accomplished here by altering the angle ρ at each unit geometry (refer to supplementary material section S2.3 and Figure S7 for further details) while keeping the values of the other independent variables constant. The programmable helical curvature depicted in Figure 7(b) is achieved by modifying the angle ρ according to $\rho = \rho + s\delta\rho$ geometric gradation parametrization with $\rho = 18^o$, $\delta\rho = 1^o$ and $m = 27$, where ρ is the initial angle, s is the number of unit geometry and $\delta\rho$ is the step size to change the ρ value. With the decrease in dihedral angle (θ), elevation of the metastructure increases as depicted in Figure 7(b(ii)-b(iv)), while following an asymmetric curvature along the longitudinal profile. The geometric parametrization scheme $\rho = \rho - s\delta\rho$ leads to a reverse nature of asymmetry with programmable helical curvature (as a function of dihedral angle, θ) as depicted in Figure 7(c) considering $\rho = 28^o$, $\delta\rho = 1^o$ and $m = 25$.

Symmetrically varying curvature about the midsection of the origami profile can be achieved following $\rho^{(i+1)} = \rho^{(i)} \pm s\delta\rho$ geometric gradation scheme, as depicted in Figure 7(d) with $\phi_2 = 25^o$, $\delta\rho = 1.5^o$ and $m = 20$. The variation of i from 0 to $\frac{m}{2}$ is provided following the gradation scheme of $\rho = \rho + s\delta\rho$, while for i from $\frac{m}{2}$ to m, the gradation is provided according to $\rho = \rho - s\delta\rho$, where m is the number of straight creases. The helical curve shows higher pitch for i varied from 0 to $\frac{m}{2}$ and lower pitch for i varied from $\frac{m}{2}$ to m. The out-of-plane curvature and elevation increase due to the folding of creases with a decrease in the dihedral angle (θ) from 150^o to 90^o (Figure 7(d(ii)-d(iv)).

The programmable helical curvature depicted in Figure 7(e) is achieved by modifying the angle ρ according to $\rho^{(i+1)} = \rho^{(i)} \mp s\delta\rho$ gradation scheme with $\phi_2 = 28^o$, $\delta\rho = 1.5^o$ and $n = 20$. The variation of i from 0 to $\frac{m}{2}$ is provided following the gradation scheme of $\rho = \rho - s\delta\rho$, while for i from $\frac{m}{2}$ to m, the gradation is provided according to $\rho = \rho + s\delta\rho$, where m is the number of straight creases. The helical curve shows lower pitch for i varied from 0 to $\frac{m}{2}$ and higher pitch for i varied from $\frac{m}{2}$ to m. The out-of-

plane curvature and elevation increase due to the folding of creases with a decrease in the dihedral angle (θ) from 150^o to 90^o (Figure 7(e(ii)-d(iv)). In general, it is noticed that the incorporation of geometric gradation can modify pitch, as well as the in and out-plane curvature of the helical architecture.

In summary, we have demonstrated that a range of symmetric and asymmetric curvatures can be achieved with unidirectional, bidirectional, and helical shapes through graded piecewise assembly of second-order Miura-ori derivatives. It is shown that planar and orthogonal rims in the helical origami architectures can be obtained from a flat 2D configuration by exploiting the folding mechanics and geometry of functionally architected creases. Further, the curvature, degree of asymmetry, elevation, diameter, and pitch can be actively programmed as a function of the dihedral angle by limited actuation exploiting the one-degree-of-freedom characteristics of the proposed origami architectures. All the proposed architectures conform to the developability criteria, demonstrating two to three dimensional shape transition characteristics.

4. Conclusions and perspective

In this paper, we have proposed second-order graded derivatives of Miura origami, leading to programmable uni and bi-directional curvatures with symmetric or asymmetric geometries. It is demonstrated that a flat sheet of material can be converted to parabolic, S shape, circular and helical curvatures with planar or orthogonal rims through minimal actuation by altering the dihedral angle of a unit cell. The curvature, degree of asymmetry, elevation, diameter and pitch can be actively programmed as a function of the folding angle of optimally selected creases exploiting the single-degree-of-freedom characteristics of the proposed origami architectures.

The conventional Miura pattern leads to in-plane deformation without any three dimensional shape morphing. We propose derivatives of the Miura geometry by strategic modifications in the unit cell that lead to achieving target curvatures, wherein the asymmetry can further be controlled through geometric gradations. The Arc Miura unit cells result in unidirectional parabolic or bi-directional S shapes, while the helical curvatures with planar and orthogonal rims are obtained by inclined Arc Miura and tapered Arc Miura unit cells respectively. It can be noted that the two-dimensional uni-directional parabolic and S-shape curvatures can further be extended to 3D metasurfaces with target curvatures, wherein a programmable control can be achieved through minimal actuation of the constituting origami rib architectures.

The rigid foldability and motion behavior of the graded geometries are investigated thoroughly based on computational simulations and tabletop experiments using physical prototypes, leading to the evidence of on-demand shape morphing under limited actuation and transitional deployment from 2D to 3D states.

An efficient approach of kinematic mapping is developed based on idealized spherical 4R linkages involving Denavit-Hartenberg matrix notations, resulting in piecewise spatially-graded tessellations for achieving programmed pre-defined symmetric and asymmetric curvatures with complex two and three-dimensional geometrical shapes. The proposed framework of graded Miura origami derivatives is generic in nature, and it can be extended to achieve any pre-defined curves and metasurfaces with multiple curvatures having different degrees through incorporating appropriate gradation schemes, wherein inverse optimization can be readily exploited.

Real-time programmable mechanical features including shape morphing ability in metamaterials and metasurfaces can be crucial for a range of advanced space applications such as adaptive solar arrays, deployable space structures and antennas, robotic arms, actuators and advanced robotic materials. For example, precise control over the curvature and geometric parameters of the origami structure can enable a wide range of frequencies, flexible variation of radiation properties, and the ability to switch polarisation states, making these designs highly adaptable for advanced space communication systems and re-configurable antenna designs. The fundamental mechanics of the proposed origami metamaterials being mostly scale-independent, this rapidly emerging class of deployable shape-changing architectures can be directly transferred for application in a range of milli-, micro-, and nanometre-size space systems, essentially opening avenues for the design of various programmable mechanical and aerospace structures at multiple length-scales.

5. Methods

5.1. Computational methods

Kinematic and geometric analyses of Arc Miura, inclined Arc Miura and tapered Arc Miura are carried out to obtain programmed uniform and graded tessellations of symmetric and asymmetric curvatures such as unidirectional curvature, S curvature and helical curvature with planar and orthogonal rims. The detailed computational formulation is provided in the supplementary material.

5.2. Physical experiments

Besides extensive computational analyses, we have prepared physical prototypes of selected configurations to demonstrate the programmable on-demand shape morphing characteristics of a range of symmetric and asymmetric curvatures such as unidirectional, bidirectional S and helical geometries. For the physical experiments, the material used is 300 GSM thickness origami flat sheets with dimensions 12×18 inches that can be easily cut into desired shapes. The creases are created using CAD packages and automated scoring machines before folding according to the valley and mountain patterns. The

qualitative motion behaviour of the origami architectures is captured using a high-quality camera based on tabletop experiments.

Supplementary materials

Supplementary sections:

S1: Kinematic analysis of unit geometry

S2: Geometric analysis of uniform and graded tessellations

Supplementary figures: Figures S1 to S7

Acknowledgements

TM would like to acknowledge the Initiation grant received from University of Southampton during the period of this research work.

Data Availability

All data used in this paper to present the results can be made available upon reasonable request to the corresponding author.

Conflicts of Interest

The authors declare no conflicts of interest.

Author Contributions

TM conceived the idea and strategy for computational model development. AS carried out the derivations and prepared the figures under the supervision of TM and SN. All the authors contributed equally in preparing the manuscript.

References

[1] P. Sinha, T. Mukhopadhyay, Programmable multi-physical mechanics of mechanical metamaterials, Materials Science and Engineering: R: Reports 155 (2023) 100745.

[2] P. Sinha, T. Mukhopadhyay, Pneumatic elastostatics of multi-functional inflatable lattices: realization of extreme specific stiffness with active modulation and deployability, Royal Society Open Science 11 (2) (2024) 231272.

[3] D. Kundu, T. Mukhopadhyay, Pneumatic optimally-tapered inflatable lattices with deployable and conformal characteristics, Space: Science & Technology.

[4] R. E. Skelton, J. W. Helton, R. Adhikari, J.-P. Pinaud, W. Chan, An introduction to the mechanics of tensegrity structures, in: The mechanical systems design handbook, 2017, pp. 315–388.

[5] B. Wang, J. Zhu, S. Zhong, W. Liang, C. Guan, Space deployable mechanics: A review of structures and smart driving, Materials & Design 237 (2024) 112557.

[6] A. Sharma, S. Naskar, T. Mukhopadhyay, Multi-physically programmable tubular origami metamaterials: Exploitable nexus of geometry, folding mechanics and stimuli-responsive physics, Advanced Science (2025) e05089.

[7] H. Fei, W. Lei, L. Shiyang, D. Zichen, Energy-preserving perturbation method for thermally induced dynamics in aerospace tensegrity structures, AIAA Journal (2024) 1–14.

[8] H. Zou, L. Wu, W. Li, F. Han, Z. Deng, Thermally-induced vibration analysis of tensegrity modules during space deployment using dynamic stiffness method, International Journal of Solids and Structures 282 (2023) 112454.

[9] A. Sharma, S. Naskar, T. Mukhopadhyay, Programmable constitutive mode-coupling in tubular origami metamaterials, npj Metamaterials (2025).

[10] A. Tiwari, S. Upadhyay, T. Mukhopadhyay, On introducing conicity in tubular origami metastructures for programming the nonlinear dynamics in an expanded design space, Journal of Sound and Vibration 603 (2025) 118941.

[11] Z. Zhai, L. Wu, H. Jiang, Mechanical metamaterials based on origami and kirigami, Applied Physics Reviews 8 (4) (2021) 041319.

[12] A. Gillman, G. Wilson, K. Fuchi, D. Hartl, A. Pankonien, P. Buskohl, Design of soft origami mechanisms with targeted symmetries, Actuators 8 (2018) 3.

[13] Y.-K. Lee, J. Kim, J.-M. Lien, Y.-J. Lee, I.-S. Choi, Recent progress in shape-transformable materials and their applications, Electronic Materials Letters 18 (3) (2022) 215–231.

[14] S. Li, H. Fang, S. Sadeghi, P. Bhovad, K.-W. Wang, Architected origami materials: how folding creates sophisticated mechanical properties, Advanced materials 31 (5) (2019) 1805282.

[15] S. J. Callens, A. A. Zadpoor, From flat sheets to curved geometries: Origami and kirigami approaches, Materials Today 21 (3) (2018) 241–264.

[16] Y. Chen, J. Yan, J. Feng, Geometric and kinematic analyses and novel characteristics of origami-inspired structures, Symmetry 11 (2019) 1101.

[17] A. Sinha, T. Mukhopadhyay, Kirigami-inspired metamaterials for programming constitutive laws: Mixed-mode multidirectional auxeticity and contact-induced stiffness modulation, iScience 25 (12) (2022) 105656.

[18] Z. Zhai, Y. Wang, K. Lin, L. Wu, H. Jiang, In situ stiffness manipulation using elegant curved origami, Science advances 6 (47) (2020) eabe2000.

[19] Z. Wo, E. T. Filipov, Stiffening multi-stable origami tubes by outward popping of creases, Extreme Mechanics Letters 58 (2023) 101941.

[20] C. M. Andres, J. Zhu, T. Shyu, C. Flynn, N. A. Kotov, Shape-morphing nanocomposite origami, Langmuir 30 (19) (2014) 5378–5385.

[21] H. Chen, X.-L. Zhang, Y.-Y. Zhang, D. Wang, D.-L. Bao, Y. Que, W. Xiao, S. Du, M. Ouyang, S. T. Pantelides, et al., Atomically precise, custom-design origami graphene nanostructures, Science 365 (6457) (2019) 1036–1040.

[22] J. Cai, E. Estakhrianhaghighi, A. Akbarzadeh, Functionalized graphene origami metamaterials with tunable thermal conductivity, Carbon 191 (2022) 610–624.

[23] Z. Chen, B. Tighe, J. Zhao, Origami-inspired modules enable a reconfigurable robot with programmable shapes and motions, IEEE/ASME Transactions on Mechatronics 27 (4) (2022) 2016–2025.

[24] Y. Park, J. Kang, Y. Na, Reconfigurable shape morphing with origami-inspired pneumatic blocks, IEEE Robotics and Automation Letters 7 (4) (2022) 9453–9460.

[25] C. Wang, H. Guo, R. Liu, Z. Deng, Y. Chen, Z. You, Reconfigurable origami-inspired multistable metamorphous structures, Science Advances 10 (22) (2024) eadk8662.

[26] Q. Ze, S. Wu, J. Nishikawa, J. Dai, Y. Sun, S. Leanza, C. Zemelka, L. S. Novelino, G. H. Paulino, R. R. Zhao, Soft robotic origami crawler, Science advances 8 (13) (2022) eabm7834.

[27] P. Sareh, P. Chermprayong, M. Emmanuelli, H. Nadeem, M. Kovac, Rotorigami: A rotary origami protective system for robotic rotorcraft, Science Robotics 3 (22) (2018) eaah5228.

[28] M. Meloni, J. Cai, Q. Zhang, D. Sang-Hoon Lee, M. Li, R. Ma, T. E. Parashkevov, J. Feng, Engineering origami: A comprehensive review of recent applications, design methods, and tools, Advanced Science 8 (13) (2021) 2000636.

[29] R. Xie, D. Hou, J. Ma, Y. Chen, Z. You, Geometrically graded origami tubes, in: International Design Engineering Technical Conferences and Computers and Information in Engineering Conference, Vol. 50169, American Society of Mechanical Engineers, 2016, p. V05BT07A010.

[30] J. Chung, M. Song, S.-H. Chung, W. Choi, S. Lee, Z.-H. Lin, J. Hong, S. Lee, Triangulated cylinder origami-based piezoelectric/triboelectric hybrid generator to harvest coupled axial and rotational motion, Research (2021) 7248579.

[31] S. Yao, X. Liu, S. V. Georgakopoulos, Morphing origami conical spiral antenna based on the nojima

wrap, IEEE Transactions on Antennas and Propagation 65 (5) (2017) 2222–2232.

[32] M. Schenk, A. D. Viquerat, K. A. Seffen, S. D. Guest, Review of inflatable booms for deployable space structures: packing and rigidization, Journal of Spacecraft and Rockets 51 (3) (2014) 762–778.

[33] H. Sharma, Folding pattern design and deformation behavior of origami based conical structures, Advances in Space Research 67 (7) (2021) 2058–2076.

[34] H. Sharma, S. H. Upadhyay, Geometric design and deployment behavior of origami inspired conical structures, Mechanics Based Design of Structures and Machines 51 (1) (2023) 113–137.

[35] Q. Chen, F. Feng, P. Lv, H. Duan, Origami spring-inspired shape morphing for flexible robotics, Soft Robotics 9 (4) (2022) 798–806.

[36] J. Cui, F. R. Poblete, Y. Zhu, Origami/kirigami-guided morphing of composite sheets, Advanced Functional Materials 28 (44) (2018) 1802768.

[37] J. Xu, C. Fu, Q. Fu, Y. Chen, Y. Ma, X. Feng, Flexible arc-armor inspired by origami, International Journal of Mechanical Sciences 201 (2021) 106463.

[38] X. Xiang, G. Lu, Z. You, Energy absorption of origami inspired structures and materials, Thin-Walled Structures 157 (2020) 107130.

[39] T. Mukhopadhyay, J. Ma, H. Feng, D. Hou, J. M. Gattas, Y. Chen, Z. You, Programmable stiffness and shape modulation in origami materials: Emergence of a distant actuation feature, Applied Materials Today 19 (2020) 100537.

[40] Y. Zhao, S. Li, M. Zhang, L. Zeng, Y. Yang, Y. Kanamori, J. Mitani, Computational design methods for cylindrical and axisymmetric waterbomb tessellations, Computer Aided Geometric Design 91 (2021) 102037.

[41] J. Zhang, S. Liu, L. Zhang, C. Wang, Origami-based metasurfaces: Design and radar cross section reduction, AIAA Journal 58 (12) (2020) 5478–5482.

[42] A. Meeussen, M. van Hecke, Multistable sheets with rewritable patterns for switchable shape-morphing, Nature 621 (7979) (2023) 516–520.

[43] R. M. Neville, F. Scarpa, A. Pirrera, Shape morphing kirigami mechanical metamaterials, Scientific reports 6 (1) (2016) 31067.

[44] C. Jiang, F. Rist, H. Wang, J. Wallner, H. Pottmann, Shape-morphing mechanical metamaterials, Computer-Aided Design 143 (2022) 103146.

[45] A. Karami, A. Reddy, H. Nassar, Curved-crease origami for morphing metamaterials, Physical Review Letters 132 (10) (2024) 108201.

[46] S. Wang, P. Yan, H. Huang, N. Zhang, B. Li, Inflatable metamorphic origami, Research 6 (2023)

0133.

[47] K. Liu, F. Hacker, C. Daraio, Robotic surfaces with reversible, spatiotemporal control for shape morphing and object manipulation, Science Robotics 6 (53) (2021) eabf5116.

[48] F. Wang, H. Gong, X. Chen, C. Chen, Folding to curved surfaces: A generalized design method and mechanics of origami-based cylindrical structures, Scientific reports 6 (1) (2016) 33312.

[49] Z. Liu, H. Fang, J. Xu, K. Wang, A novel origami mechanical metamaterial based on miura-variant designs: exceptional multistability and shape reconfigurability, Smart Materials and Structures 30 (8) (2021) 085029.

[50] S. Park, E. Park, M. Lee, S. Lim, Shape-morphing antenna array by 4d-printed multimaterial miura origami, ACS applied materials & interfaces 15 (42) (2023) 49843–49853.

[51] S. W. Grey, F. Scarpa, M. Schenk, Embedded actuation for shape-adaptive origami, Journal of Mechanical Design 143 (8) (2021) 081703.

[52] T. Tachi, Generalization of rigid-foldable quadrilateral-mesh origami, Journal of the International Association for Shell and Spatial Structures 50 (3) (2009) 173–179.

[53] K. Miura, Map fold a la miura style, its physical character and application to the space science, in: Proceedings of the First International Meeting of Origami Science and Technology, Ferrara, 1989, pp. 39–49.

[54] D. Misseroni, P. P. Pratapa, K. Liu, B. Kresling, Y. Chen, C. Daraio, G. H. Paulino, Origami engineering, Nature Reviews Methods Primers 4 (1) (2024) 40.

[55] L. H. Dudte, E. Vouga, T. Tachi, L. Mahadevan, Programming curvature using origami tessellations, Nature materials 15 (5) (2016) 583–588.

[56] R. Lang, P. Wang-Iverson, M. Yim, Origami 5: Fifth International Meeting of Origami Science, Mathematics, and Education, 2016.

[57] I. a. N. De Temmerman, M. Mollaert, I. a. T. Van Mele, I. a. L. De Laet, Design and analysis of a foldable mobile shelter system, International Journal of Space Structures 22 (3) (2007) 161–168.

[58] A. Kuenstler, M. Trautz, Deployable folding patterns using stiff plate elements., Bautechnik 88 (2) (2011) 86–93.

[59] F. Gioia, D. Dureisseix, R. Motro, B. Maurin, Design and analysis of a foldable/unfoldable corrugated architectural curved envelop, Journal of Mechanical Design 134 (2012) 031003.

[60] Q. Zhang, X. Wang, D. S.-h. Lee, J. Cai, Z. Ren, J. Feng, Development of kinetic origami canopy using arc miura folding patterns, Journal of Building Engineering 43 (2021) 103116.

[61] F. Albermani, H. Khalilpasha, H. Karampour, Propagation buckling in deep sub-sea pipelines, En-

gineering Structures 33 (9) (2011) 2547–2553.

[62] L. Yuan, H. Shi, J. Ma, Z. You, Quasi-static impact of origami crash boxes with various profiles, Thin-Walled Structures 141 (2019) 435–446.

[63] C. A. Velez, A.-S. Kaddour, S. V. Georgakopoulos, D. S. Bolanos, C. Ynchausti, S. Magleby, L. L. Howell, Reconfigurable and deployable miura-ori ra analysis for satellite applications, in: 2021 IEEE 21st Annual Wireless and Microwave Technology Conference (WAMICON), IEEE, 2021, pp. 1–3.

[64] Y. Meng, W. Yang, Y. Yu, X. Cheng, J. Zhiwei, A crawling soft robot driven by pneumatic foldable actuators based on miura-ori, Actuators 9 (2020) 26.

[65] M. Schenk, S. D. Guest, Geometry of miura-folded metamaterials, Proceedings of the National Academy of Sciences 110 (9) (2013) 3276–3281.

[66] E. T. Filipov, T. Tachi, G. H. Paulino, Origami tubes assembled into stiff, yet reconfigurable structures and metamaterials, Proceedings of the National Academy of Sciences 112 (40) (2015) 12321–12326.

[67] J. Cai, X. Deng, J. Feng, Y. Zhou, Geometric design and mechanical behavior of a deployable cylinder with miura origami, Smart Materials and Structures 24 (12) (2015) 125031.

[68] Y. Hu, Y. Zhou, H. Liang, Constructing rigid-foldable generalized miura-ori tessellations for curved surfaces, Journal of Mechanisms and Robotics 13 (1) (2021) 011017.

[69] L. H. Dudte, E. Vouga, T. Tachi, L. Mahadevan, Programming curvature using origami tessellations, Nature materials 15 (5) (2016) 583–588.

[70] Y. Hu, H. Liang, H. Duan, Design of cylindrical and axisymmetric origami structures based on generalized miura-ori cell, Journal of Mechanisms and Robotics 11 (5) (2019) 051004.

[71] Z. Li, Q. Yang, R. Fang, W. Chen, H. Hao, Origami metamaterial with two-stage programmable compressive strength under quasi-static loading, International Journal of Mechanical Sciences 189 (2021) 105987.

[72] H. Wang, D. Zhao, Y. Jin, M. Wang, T. Mukhopadhyay, Z. You, Modulation of multi-directional auxeticity in hybrid origami metamaterials, Applied Materials Today 20 (2020) 100715.

[73] Y. Lv, Y. Zhang, N. Gong, Z.-x. Li, G. Lu, X. Xiang, On the out-of-plane compression of a miura-ori patterned sheet, International Journal of Mechanical Sciences 161 (2019) 105022.

[74] H. Fang, S. Li, H. Ji, K. Wang, Dynamics of a bistable miura-origami structure, Physical Review E 95 (5) (2017) 052211.

[75] J. M. Gattas, Z. You, Miura-base rigid origami: parametrizations of curved-crease geometries, Journal of Mechanical Design 136 (12) (2014) 121404.

[76] Y. Liu, W. Zhang, F. Zhang, X. Lan, J. Leng, S. Liu, X. Jia, C. Cotton, B. Sun, B. Gu, et al., Shape memory behavior and recovery force of 4d printed laminated miura-origami structures subjected to compressive loading, Composites Part B: Engineering 153 (2018) 233–242.

[77] J. M. Gattas, W. Wu, Z. You, Miura-base rigid origami: parameterizations of first-level derivative and piecewise geometries, Journal of Mechanical design 135 (11) (2013) 111011.

[78] V. Khaliulin, A technique for synthesizing the structures of folded cores of sandwich panels, Izvestiya Vysshikh Uchebnykh Zavedenij Aviatsionnaya Tekhnika 48 (2005) 7–12.

[79] J. S. Beggs, Kinematics, CRC Press, 1983.

[80] Y. Zhu, M. Schenk, E. T. Filipov, A review on origami simulations: From kinematics, to mechanics, toward multiphysics, Applied Mechanics Reviews 74 (3) (2022) 030801.

[81] J. Dai, J. Rees, Mobility in metamorphic mechanisms of foldable/erectable kinds, Journal of Mechanical Design 121 (1999) 375–382.

[82] L. Paquete, Erik d. demaine and joseph o'rouke, review of geometric folding algorithms: Linkages, origami, polyhedra , cambridge university press (2007)., European Journal of Operational Research 199 (2009) 311–313.

[83] H. Stachel, A kinematic approach to kokotsakis meshes, Computer Aided Geometric Design 27 (6) (2010) 428–437.

[84] S. Liu, W. Lv, Y. Chen, G. Lu, Deployable prismatic structures with rigid origami patterns, Journal of Mechanisms and Robotics 8 (3) (2016) 031002.

[85] Y. Chen, W. Lv, J. Li, Z. You, An extended family of rigidly foldable origami tubes, Journal of Mechanisms and Robotics 9 (2) (2017) 021002.

[86] J. Cai, Z. Qian, C. Jiang, J. Feng, Y. Xu, Mobility and kinematic analysis of foldable plate structures based on rigid origami, Journal of Mechanisms and Robotics 8 (6) (2016) 064502.

[87] G. Wei, J. S. Dai, Geometry and kinematic analysis of an origami-evolved mechanism based on artmimetics, in: 2009 ASME/IFToMM International Conference on Reconfigurable Mechanisms and Robots, IEEE, 2009, pp. 450–455.